

MASS-TO-LIGHT RATIOS OF FIELD EARLY-TYPE GALAXIES AT $Z \sim 1$ FROM ULTRA-DEEP SPECTROSCOPY: EVIDENCE FOR MASS-DEPENDENT EVOLUTION¹

A. VAN DER WEL², M. FRANX², P.G. VAN DOKKUM³, H.-W. RIX⁴, G.D. ILLINGWORTH⁵, AND P. ROSATI⁶
Submitted to ApJ

ABSTRACT

We present an analysis of the Fundamental Plane for a sample of 27 field early-type galaxies in the redshift range $0.6 < z < 1.15$ in the Chandra Deep Field-South and the field of the background cluster RDCS 1252.9-2927. Sixteen of the galaxies are at $z > 0.95$. The galaxies in this sample have high signal-to-noise spectra obtained at the Very Large Telescope and high resolution imaging from the HST Advanced Camera for Surveys. From comparison with lower redshift data, we find that the mean evolution of the mass-to-light ratio (M/L) of our sample is $\Delta \ln(M/L_B) = (-1.75 \pm 0.16)z$, with a large galaxy-to-galaxy scatter. This value can be too low by 0.3 due to selection effects, resulting in $\Delta \ln(M/L_B) = (-1.43 \pm 0.16)z$. The strong correlation between M/L and rest-frame color indicates that the observed scatter is not due to measurement errors, but due to intrinsic differences between the stellar populations of the galaxies, such that our results can be used as a calibration for converting luminosities of high redshift galaxies into masses. This pace of evolution is much faster than the evolution of cluster galaxies. However, we find that the measured M/L evolution strongly depends on galaxy mass. For galaxies with masses $M > 2 \times 10^{11} M_\odot$, we find no significant difference between the evolution of field and cluster galaxies: $\Delta \ln(M/L_B) = (-1.20 \pm 0.17)z$ for field galaxies and $\Delta \ln(M/L_B) = (-1.12 \pm 0.06)z$ for cluster galaxies. The relation between the measured M/L evolution and mass is partially due to selection effects, as the galaxies are selected by luminosity, not mass. However, even when taking selection effects into account, we still find a relation between M/L evolution and mass, which is most likely caused by a lower mean age and a larger intrinsic scatter for low mass galaxies. Results from lensing early-type galaxies, which are mass-selected, show a very similar trend with mass. This, combined with our findings, provides evidence for down-sizing, i.e., for the proposition that low mass galaxies are younger than high mass galaxies. Previous studies of the rate of evolution of field early-type galaxies found a large range of mutually exclusive values. We show that these differences are largely caused by the differences between fitting methods: most literature studies are consistent with our result and with one another when using the same method. Finally, five of the early-type galaxies in our sample have AGN. There is tentative evidence that the stellar populations in these galaxies are younger than those of galaxies without AGN.

Subject headings: cosmology: observations—galaxies: evolution—galaxies: formation

1. INTRODUCTION

Understanding the formation and evolution of early-type galaxies is a key issue when addressing the mass assembly and star formation history of the galaxy population as a whole and the formation of structure in the universe, as 50% or more of all stars in the present day universe are in early-type galaxies and bulges (see, e.g., Bell et al. 2003).

In hierarchical galaxy formation theories (e.g., Cole et al. 2000), massive galaxies assemble late, such that strong evolution of the mass density from $z = 1$ to the present day is expected (see, e.g., Kauffmann & Charlot 1998). Measuring the mass density requires a measurement of the luminosity density, and an accurate determination of the M/L . M/L can be estimated from models (see, e.g., Bell et al. 2004), but these estimates are uncertain due to the age/metallicity degeneracy and the unknown IMF of the stellar populations of the galaxies (Bruzual & Charlot 2003).

The Fundamental Plane (Djorgovski & Davis 1987; Dressler et al. 1987) provides a tool to measure the evolution of M/L without model uncertainties. The M/L offset of high redshift galaxies from the local FP can be used to calibrate high red-

shift galaxy masses and to estimate the age of their stellar populations (Franx 1993). This technique has been used successfully to measure the luminosity weighted ages of massive cluster galaxies, which have formed most of their stars at redshifts $z \geq 2$ (see, e.g., van Dokkum & Franx 1996; van Dokkum & Stanford 2003, Holden et al. 2005). However, it is not clear whether galaxies in the general field evolve in the same way. In fact, in the hierarchical picture the formation redshift of galaxies with a given mass depends on environment (Diaferio et al. 2001). This would lead to substantial age differences between field and cluster galaxies at any redshift (van Dokkum et al. 2001). Since this is a generic property of all hierarchical formation models, measuring this difference is a critical test for those theories.

Various authors have measured the M/L evolution of field early-type galaxies through deep spectroscopy of magnitude limited samples. The results are much less conclusive than the results from cluster studies and the comparison between field and cluster has proved to be very hard. Some authors claim much faster evolution for field galaxies than for cluster galaxies (Treu et al. 2002; Gebhardt et al. 2003), but others find

¹ Based on observations collected at the European Southern Observatory, Chile (169.A-0458).

² Leiden Observatory, P.O.Box 9513, NL-2300 AA, Leiden, The Netherlands

³ Department of Astronomy, Yale University, P.O. Box 208101, New Haven, CT 06520-8101

⁴ Max-Planck-Institut für Astronomie, Königstuhl 17, D-69117 Heidelberg, Germany

⁵ University of California Observatories/Lick Observatory, University of California, Santa Cruz, CA 95064

⁶ European Southern Observatory, Karl-Schwarzschild-Strasse 2, D-85748 Garching, Germany

that field and cluster galaxies evolve at comparable rates (van Dokkum et al. 2001, van Dokkum & Ellis 2003, van der Wel et al. 2005). Studies involving lensing galaxies (Kochanek et al. 2000, Rusin et al. 2003, van de Ven et al. 2003), indicate the presence of a mix of fast and slowly evolving galaxies. It is unclear whether the differences between the various results are caused by selection effects, measurement errors due to low signal-to-noise spectra, low number statistics, or contamination by late-type galaxies.

This paper describes a study of early-type galaxies at $z \sim 1$ using much higher quality data than in previous studies. The substantially large number of objects with very high signal-to-noise spectra enables us to accurately measure the M/L evolution of the field early-type galaxy population, to compare the cluster and field populations, to study correlations between M/L , M , and rest-frame color, and to describe the possible effects of biases. Also, we carefully compare the samples and results from previous studies and this study in order to verify previous claims about the evolution of field galaxies, and to see whether previous results are in fact consistent with each other and these new results.

In Section 2 we describe the sample selection, the spectroscopic observations and data reduction, and the measurement of velocity dispersions. Section 3 describes the measurement of the structural parameters, colors, morphologies, and the available X-ray data. In Section 4 we present the results. Throughout this paper we use Vega magnitudes, and assume $(\Omega_M, \Omega_\Lambda) = (0.3, 0.7)$, with a Hubble constant of $H_0 = 70 \text{ km s}^{-1} \text{ Mpc}^{-1}$.

2. SPECTROSCOPY

2.1. Sample selection and Observations

We selected galaxies in the Chandra Deep Field-South (CDFS) and the RDCS1252.9-2927 cluster field (CL1252, Rosati et al. 2004), which both have deep optical imaging from the Advanced Camera for Surveys (ACS) on the HST. GOODS⁷ provides publicly available imaging in four filters (Giavalisco et al. 2004): F475W, F606W, F775W, and F850LP (hereafter b , v , i , and z). As these data were not yet available when we started this project, we used ground-based COMBO-17 photometry (Wolf et al. 2004) to select our sample for the first observing run. For subsequent runs version 0.5 of the ACS GOODS data were available, and for the last run we used the version 1.0 data release. (Blakeslee et al. 2003) provide ACS imaging on the CL1252 field in the i and z bands.

In order to construct a sample of early-type galaxies at $z \sim 1$ in the CDFS, we selected objects with $i-z > 0.86$ and COMBO-17 photometric redshifts in the range $0.8 < z_{\text{phot}} < 1.4$. (We use z when we mean 'redshift', and z_{mag} if we mean z -band magnitude, but when indicating a color we omit the mag subscript for clarity.) This color cut selects galaxies redder than a local Sbc galaxy at $z = 1$. Therefore, this study only includes galaxies that are on the red sequence at $z \sim 1$. We morphologically classified all galaxies satisfying these criteria and brighter than $z_{\text{mag}} = 21.5$, distinguishing between early- and late-type galaxies using the ACS imaging. The classification was based on compactness, regularity and the presence of spiral arms. 26 out of the 52 galaxies satisfying our selection criteria we classified as early-type galaxies. We designed multi-slit masks for three different pointings, selected by the number of primary targets that could be included. Open spaces in the masks were filled

with early-type galaxies satisfying the color and redshift criteria but fainter than $z_{\text{mag}} = 21.5$, early-type galaxies with lower photometric redshifts and late-type galaxies with $i-z > 0.85$ and redshifts $0.8 < z_{\text{phot}} < 1.4$. Switching from using ground-based $i-z$ colors from COMBO-17 to ACS $i-z$ colors from GOODS did not lead to large differences between the selected samples, although several objects changed priority.

The same selection criteria were used for the CL1252 field. However, the mask design for the CL1252 field was geometrically constrained because the primary targets were cluster galaxies at $z = 1.24$. The two brightest galaxies in the cluster are the two central galaxies, which had to be included in a single slit because of their small angular separation of $1''.5$. Therefore, not only the positions, but also the position angles of the designed masks were fixed. Unfortunately, only two galaxies brighter than $z_{\text{mag}} = 21.5$, redder than $i-z = 0.85$ and early-type morphologies could be included, additionally to the cluster galaxies. Similarly to the CDFS masks, fillers were included.

We carried out the observations with FORS2 in MXU mode on ESO's Kueyen, one of the VLT unit telescopes. We used the 600z grism together with the OG590 order separation filter to obtain a sufficiently high spectral resolution ($\sigma \approx 80 \text{ km s}^{-1}$) and to cover the wavelength range around the Balmer/4000Å break for galaxies at $z \sim 1$. The observations were carried out in series of four dithered exposures with spatial offsets of $1''.5$ or $2''$ and equal exposure times ranging from 14 to 30 minutes each.

In total, 51 hours of scientifically useful integration time was acquired, of which 38 hours had seeing better than $1''$. The cumulative integration time for the three pointings in the CDFS is 27 hours, with a median seeing of $0''.95$. The single pointing in the CL1252 field has an integration time of 24 hours, with a median seeing of $0''.65$. These observations were carried out during five different observing runs from September 2002 to November 2003.

The sample described in this paper consists of 38 galaxies with velocity dispersions, of which 20 are early-type galaxies at $z \sim 1$, and 18 are early-type galaxies at lower redshift, or late-type galaxies. 100% of our primary targets yielded velocity dispersions. The CL1252 observations also yielded four velocity dispersions of cluster galaxies. The FP of the 1252 cluster is discussed by (Holden et al. 2005).

2.2. Data Reduction

The spectroscopic data were reduced using standard IRAF tasks. Lamp flat fields were taken before or after each night, in sequences of five exposures. We used the sequence closest in time to the science observation. Cosmic rays were removed using the L.A.Cosmic task (van Dokkum 2001). Afterward, all frames were checked manually. We subtracted a two-dimensional sky spectrum from each exposure, obtained by median averaging the four dithered exposures in a sequence, masking the target and secondary or serendipitous objects, if present. The atmospheric emission lines, which are bright and abundant in the observed wavelength range, were used to perform the wavelength calibration. We corrected for distortion in the spatial direction by tracing the target. All individual exposures were optimally weighted to obtain maximum S/N .

There are various atmospheric absorption features in the observed wavelength range. Because the strength and shape of these features change with airmass and atmospheric conditions

⁷ <http://www.stsci.edu/science/goods/>

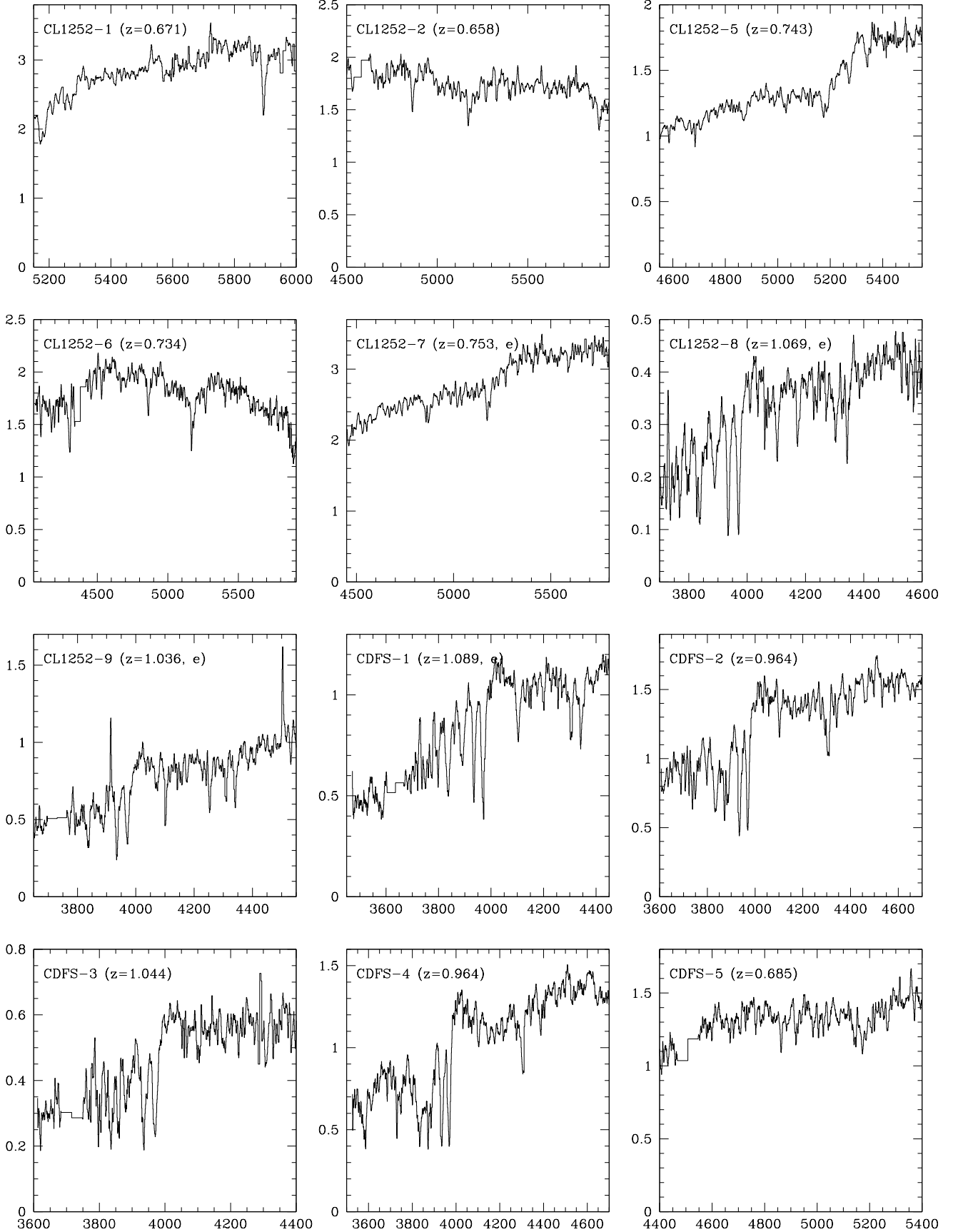


FIG. 1.— Rest-frame spectra in 8\AA bins of the galaxies in our sample with early-type morphologies, used in the analysis in the subsequent sections. The area around 7600\AA (observed wavelength) and the positions of bright skylines are excluded from the binning. The wavelength range differs from object to object due to differences in redshift and slit position. Every spectrum is labeled with the redshifts and an 'e' if the spectrum shows one or more emission lines.

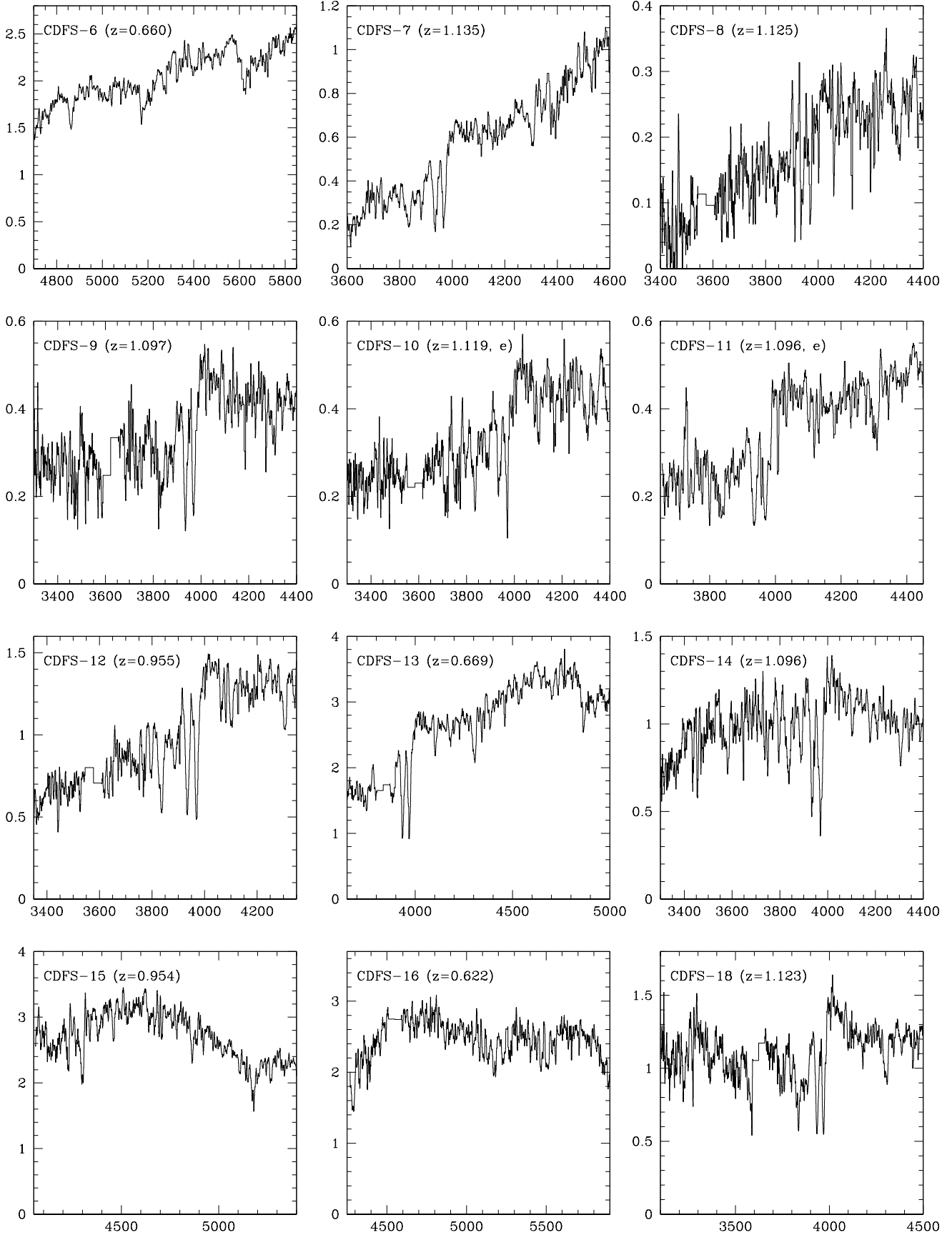


FIG. 1.— Continued

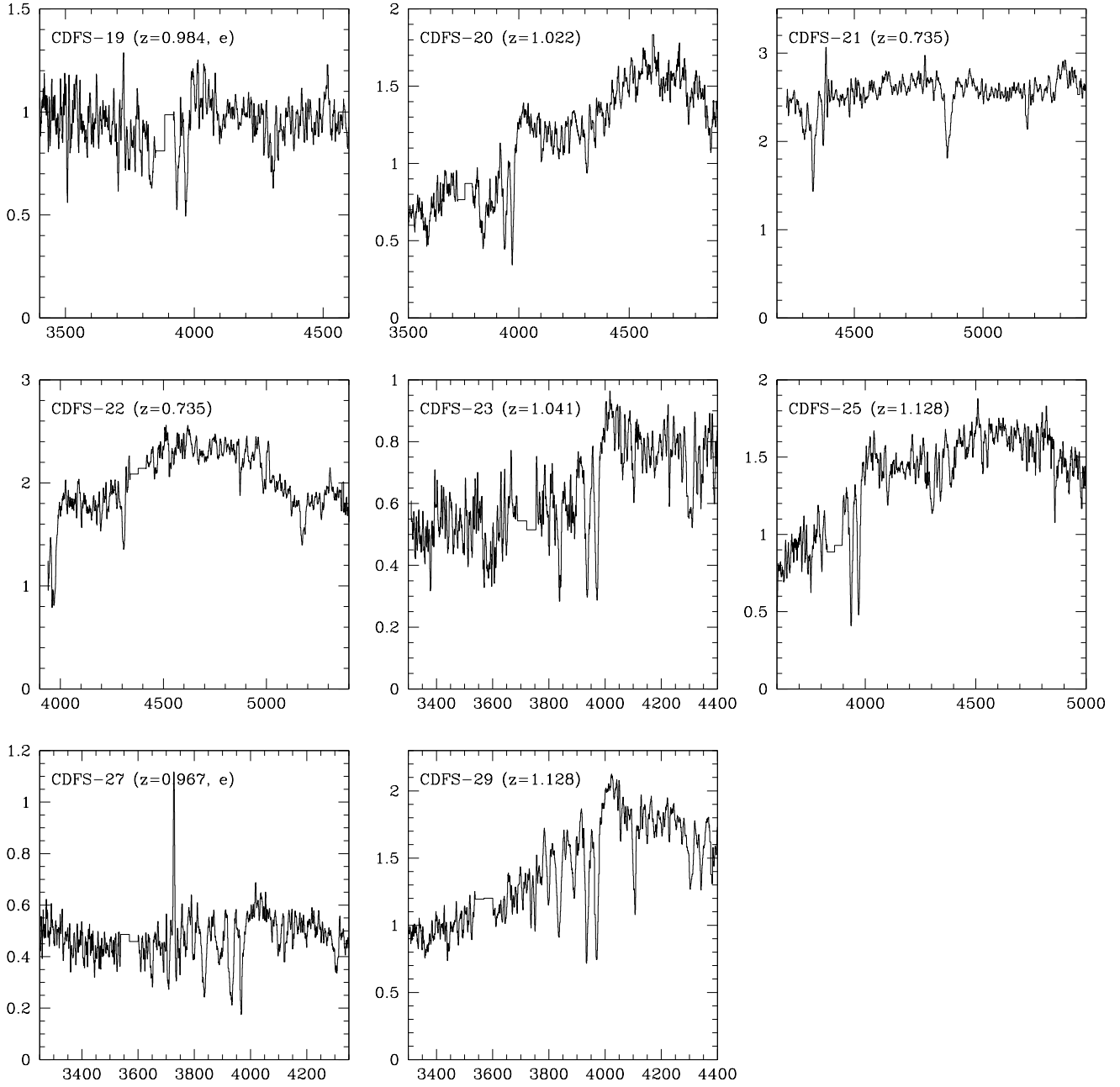


FIG. 1.— Continued

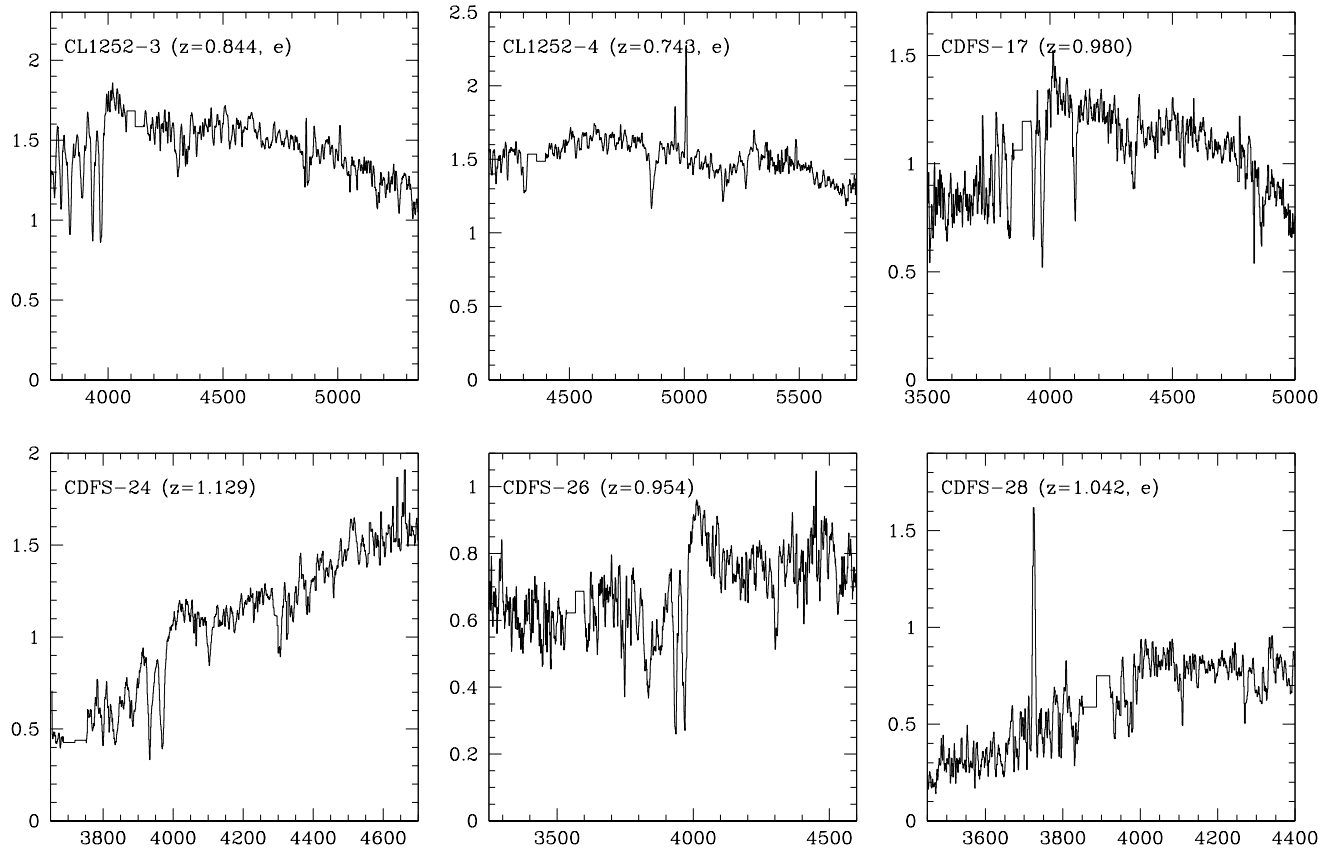


FIG. 2.— Rest-frame spectra in 8 Å bins of the galaxies in our sample with late-type and irregular morphologies. These are not included in the analysis in the subsequent sections. For further explanation of the spectra, see Figure 1.

we needed to correct each exposure separately. To this end we included a blue star in each of our masks, which was reduced along with the galaxy spectra. After the final combination, the regions in the galaxy spectra with atmospheric features were divided by the normalized spectrum of the blue star. Spectroscopic standard stars were used to do a relative flux calibration. One-dimensional spectra were extracted by adding those pixel rows with more than 25% of the flux of the brightest row, weighting optimally.

The smoothed one-dimensional spectra are shown in Figure 2. The coordinates of the objects for which we measured velocity dispersions (see Section 2.3) in Table 1. Redshifts, S/N and emission lines are given in Table 2.

2.3. Velocity Dispersions

Velocity dispersions are obtained by fitting template spectra to the observed galaxy spectra. The fitting method is extensively described by (van Dokkum & Franx 1996). The continua of both the observed and the template spectra are filtered out in Fourier space and the template spectrum is convolved with a Gaussian to match the width of the absorption lines in the galaxy spectrum. The part of the galaxy spectrum used in the fit is as large as possible. Therefore, our measurements do not rely on a few high S/N absorption features.

As templates we use Coudé spectra of 132 stars with the appropriate wavelength range from the sample constructed by (Valdes et al. 2004), with a spectral range from F0 to M6, in-

cluding both very low and high metallicity stars, and different luminosity classes. These spectra have a FWHM resolution of about 1 Å. Each stellar spectrum needs to be smoothed to each galaxy spectrum separately before being re-binned. A second order function is fitted to the width of atmospheric emission lines as a function of wavelength to obtain the spectral resolution to which the template spectra are smoothed.

When fitting the galaxy spectra, we weight with the inverse of the sky brightness, and we mask the region around the atmospheric A band at 7600 Å. The spectrum above 9300 Å is omitted because of the strong atmospheric absorption, the ever increasing brightness of the sky emission lines and the decreasing system throughput.

After performing the fit for a small number of templates, masking and weighting as described, we check the residuals from the fit. Regions with emission lines, large sky line residuals and remaining data artifacts such as cosmic ray remnants are masked if present. We then apply fit the galaxy spectrum with all template spectra. We check whether the obtained parameters change strongly if one or two strong features are masked out, but we conclude that this generally is not the case: excluding the strongest features from the fit increases the χ^2 -value but does not change the results significantly in most cases. For some spectra, however, including Balmer lines in the fit leads to different results, probably because unseen emission line contributions contaminate these features. For low quality spectra

($S/N \leq 10$ per 1.6 pixel in the extracted, one-dimensional spectra) the contributions of Balmer lines or other strong features can hardly be checked because excluding these strong features leaves insufficient signal to obtain a proper fit. Therefore, we exclude objects with $S/N < 12$ spectra from our analysis, but we mention the effect of including these.

For all spectra with $S/N \geq 12$ the random errors are below 3% for $\sigma > 200 \text{ km s}^{-1}$, and below 5% for $\sigma < 200 \text{ km s}^{-1}$. Adding a systematic uncertainty (including template mismatch and the error on the resolution of the galaxy spectra) of about 10% for $S/N = 10$ spectra and 2% for the highest S/N spectra the total errors range from 3% to 17% with a median of 7.5% for our sample of early-type galaxies with $S/N \geq 12$. Some galaxies have measured velocity dispersions that are not much larger than the resolution of the spectra. Although these are included in the analysis, they play no important role in the derivation of our results.

The best fitting stellar spectral type and the measured velocity dispersion are listed in Table 1. These velocity dispersions are aperture corrected to a $3''/4$ diameter circular aperture at the distance of Coma as described by (Jørgenson, Franx, & Kjaergaard 1995). This correction ranges from 5% to 7%.

3. PHOTOMETRY

3.1. Profile Fitting and Morphologies

The ACS provides us with an unprecedented combination of deep and high resolution imaging. The spatial resolution (FWHM) at $z = 1$ is 0.8kpc, allowing us to accurately measure the effective radii of early-type galaxies at this redshift, which typically are a few kpc. We use the single, unstacked, flat-fielded frames publicly available through the HST MAST archive. For the CDFS the number of frames for different positions ranges from 8 to 24 (with 530s exposure time each). For the CL1252 field the number of frames ranges from 10 to 40 (with 1200s exposure time each), but is mostly 10 as only the center of the cluster has 40 overlapping images.

For each galaxy each individual z band image is fitted by $r^{1/n}$ -models (with $n = 1, 2, 3, 4$) convolved by a position dependent PSF created with TinyTim (Krist 1995), measuring r_{eff} (the effective radius), μ_{eff} (the surface brightness at r_{eff}), the position angle and the ellipticity. Each individually derived set of model parameters is distortion corrected by calculating the pixel scales in the x - and y -directions, using the polynomial distortion coefficients available through the WWW⁸. We then average the results and compute the measurement error from the scatter. The error is generally about 6% in r_{eff} , but the combination of the uncertainty in r_{eff} and μ_{eff} is such that it is directed almost parallel to the local FP. The error relevant to the offset from the FP is typically 2%. Thus, uncertainties in the offset from the local FP are dominated by the uncertainty in σ , of which the error is pointed almost perpendicular to the FP. The effective radii and surface brightnesses are given in Table 1. For consistency with earlier studies, these are the values obtained from fitting a de Vaucouleur profile in our analysis.

To transform the observed z band surface brightnesses to the rest-frame B band, we use the technique described by (van Dokkum & Franx 1996), using the templates from (Coleman, Wu, & Weedman 1980) and observed colors (see Section 3.2) to interpolate between the pass-bands. The calculated rest-frame

B band surface brightnesses only depend very weakly on the spectral type of the template used. The typical difference found for using the Sbc template instead of the E template is less than 0.02 mag. The transformations are a function of redshift. As an example we give the transformation (based on the E template) for a galaxy at $z = 1$:

$$B_z = z + 0.165(i - z) + 1.398 \quad (1)$$

Physical sizes and rest-frame B -band surface brightnesses are given in Table 3.

Figures 3 and 4 show the combined residuals of the $r^{1/4}$ -fits along with the color images of the 38 galaxies with velocity dispersions. Figure 3 shows the early-type galaxies, Figure 4 the late-type galaxies. Two numbers are used to characterize the magnitude of the residuals. At the upper right of each residual image the absolute value of the flux in the asymmetric part of the residual is given as a percentage of the total flux of the galaxy, obtained by subtracting the residual rotated by 180 degrees from the residual itself. In the upper left the absolute value of the flux in the symmetric part of the residual is given as a percentage of the total flux of the galaxy. We find that the asymmetric residual is a good indicator of morphology. Our final morphological qualification is a combination of the magnitude of the asymmetric residual and visual inspection of the cause of the asymmetry. Some of the early-type galaxies (Figure 3) have significant asymmetric residuals, but these are caused by features on a very small scale, in the centers of the galaxies, i.e. not by features attributed to spiral arms or other large scale irregularities. The late-type galaxies (Figure 4) have large asymmetric residuals, caused by large scale structures like spiral arms. We note that the Sercic number does not distinguish well between late- and early-type galaxies. For example, the most massive galaxy in our sample has $n=2$ and some galaxies that we classify as late-type galaxies have $n=4$.

3.2. Colors

We supplement the ACS imaging with ground-based optical and near-IR imaging from FORS2 and ISAAC on the VLT and SOFI on the NTT (Vandame et al., in preparation). GOODS ACS imaging of the CDFS provides photometry in the b , v , i , and z bands (data release version 1.0), and ESO's imaging survey⁹ provides SOFI and ISAAC imaging in the J and K bands. Since the CDFS is not entirely covered by ISAAC we use the SOFI data for the objects outside the ISAAC pointings. All images were smoothed to match the resolution of the K band data with the worst seeing, which is $0''.8$ for the ISAAC imaging and $1''$ for the SOFI imaging. The photometric differences between the ISAAC and SOFI datasets are small (< 0.01 mag), since the zero-points of the ISAAC data are based on SOFI photometry. For the CL1252 field we use optical imaging from ACS (i and z) and FORS2 (B , V , and R) and near-IR imaging from ISAAC (Lidman et al. 2004). Again, all images were smoothed to match the ground-based data with the worst seeing, which is $0''.6$ in the B band.

We measure the flux in each band for each of our spectroscopic targets within several apertures with different radii ($1/2/3r_{eff}$ and $0''.8$). Contaminating objects within the aperture are masked. We choose to use the fluxes measured within a radius of $2r_{eff}$, with a minimum of $0''.8$, trading off between the measurement accuracy and the amount of contamination.

⁸ <http://www.stsci.edu/hst/acs/analysis/PAMS>

⁹ <http://www.eso.org/science/eis/>

The $i-z$ and $J-K$ colors are given in Table 2, as well as total *AUTO* z band and K band magnitudes, as obtained with SExtractor (Bertin & Arnouts 1996).

The availability of near-IR photometry not only allows us to compute rest-frame $U-B$ colors, but also rest-frame $B-I$ colors. To transform the observed colors to rest-frame $U-B$ and $B-I$ we use the same method as used to calculate rest-frame B band surface brightnesses (see Section 3.2). For $z=1$, using the E template, the transformation is:

$$(U-B)_z = 0.836(i-z) + 0.276(v-i) - 1.111 \quad (2)$$

$$(B-I)_z = z - K + 0.165(i-z) - 0.513(J-K) - 0.282 \quad (3)$$

Rest-frame colors are given in Table 3.

3.3. X-ray Data

For both the CDFS and the CL1252 field deep X-ray data from Chandra are available, such that we can check for the presence of AGN in our galaxy sample. Giacconi et al. (2002) and Alexander et al. (2003) provide catalogs of the CDFS data. The Chandra data of the CL1252 field is described by (Rosati et al. 2004), who also constructed a point source catalog. Eight galaxies in our sample of 38 are identified as AGN, based on their large X-ray luminosities (typically $> 10^{42} \text{ erg s}^{-1}$). Five of these are early-type galaxies, of which two have emission lines in their spectra. Besides the eight AGN, two galaxies in our sample are identified as extended X-ray sources. This X-ray radiation is accounted for by diffuse halo gas. The X-ray luminosities of CDFS-4 and CDFS-22 are $7.15 \times 10^{41} \text{ erg s}^{-1}$ and $3.42 \times 10^{42} \text{ erg s}^{-1}$, respectively. It is not surprising that CDFS-4 and CDFS-22 turn out to be two of the most massive galaxies in our sample. Also, CDFS-22 is one of the galaxies with an AGN. The X-ray properties of our sample of galaxies are given in Table 2.

4. MASSES, MASS-TO-LIGHT RATIOS AND STELLAR POPULATIONS OF EARLY-TYPE GALAXIES AT $z=1$

4.1. The Fundamental Plane

Jørgensen, Franx, & Kjaergaard (1996) have shown that the FP for cluster galaxies in the local universe can be described by

$$\log R_{\text{eff}} = 1.2 \log \sigma - 0.83 \log I_{\text{eff},B} + \gamma, \quad (4)$$

where R_{eff} is the effective radius in kpc, σ the central velocity dispersion in km s^{-1} , $I_{\text{eff},B}$ the surface brightness in the B band ($\log I_{\text{eff},B} = -0.4 \mu_{B_z}$), and γ the intercept. The values of the coefficients are derived from the early-type galaxies in ten nearby clusters, and imply that mass and M/L scale as $M/L_B \propto M^{0.28}$. From the sample of Faber et al. (1989) we derived that the intercept of the FP lies lower by 0.04 in the projection given above. The offsets of the high- z galaxies are computed using a local FP with coefficients from Jørgensen et al. (1996) but with the intercept derived from the Faber et al. (1989) sample.

Besides the form of the local FP, we need a large sample of local field early-type galaxies, for example to address issues such as selection effects. We construct our local field sample as in Bernardi et al. (2003): we take early-type galaxies from the Sloan Digital Sky Survey and include those with less than 10 neighbors brighter than $M_i = -20.55$ and closer than $1.4 Mpc$. We convert the rest-frame g and r band surface brightnesses to a B band surface brightness using the conversion given by Jørgensen et al. (1996). As we need the surface brightness in the g and r bands at the same radius, and Bernardi et al. derive

effective radii separately for each band, we compute the surface brightness in the r band at the effective radius as measured in the g band. We note that the FP coefficients as derived by Bernardi et al. are different from those from Jørgensen et al., but this does not lead to different results.

In Figure 5 we show the FP of the SDSS galaxies and our sample, where the surface brightnesses of all galaxies are transformed to the value they would have at $z=1$, assuming luminosity evolution found for massive cluster galaxies, $\Delta \ln(M/L_B) = -1.12z$. This value for the M/L evolution of massive cluster galaxies is derived from compiling all existing data in the literature for galaxies more massive than $M = 2 \times 10^{11} M_\odot$ (van Dokkum & Franx 1996; Kelson et al. 2000; van Dokkum & Stanford 2003; Wuyts et al. 2004; Holden et al. 2005). Our field sample shown in Figure 5 includes all early-type galaxies with spectra with $S/N \geq 12$. This is also the sample used in the analysis throughout the rest of the paper, and in the subsequent figures. As can be seen, the FP already existed at $z=1$ for a large range in size. At low masses outliers occur, but the interpretation is not straightforward, as selection effects play a major role in this regime (see Section 4.3).

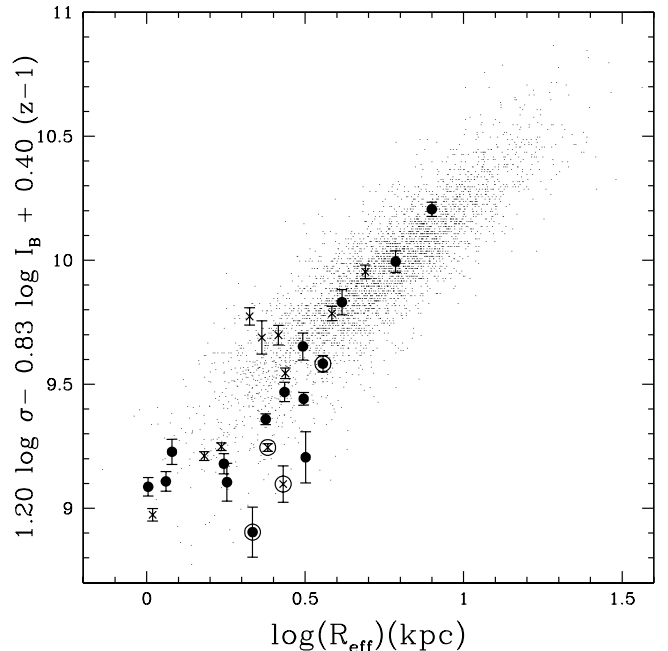


FIG. 5.— The Fundamental Plane of our sample of early-type galaxies compared to the field early-type galaxy sample from SDSS (small dots, Bernardi et al. 2003). The primary sample, early-type galaxies at $z \sim 1$ that satisfy all of our selection criteria, are indicated by the filled symbols. The crosses are fillers, mainly galaxies at redshifts $z \sim 0.7$. Encircled objects have one or more emission lines in their spectra. The surface brightness, I_B , of every galaxy in this figure is corrected for evolution to a value it would have at $z=1$, assuming $\Delta \ln(M/L_B) = -1.12z$, which is the evolution of massive cluster galaxies. The FP already existed at $z=1$ for a large range in size.

4.2. Evolution of M/L with redshift

The offset of high redshift galaxies from the local FP is interpreted as a difference in M/L as compared to equally massive local galaxies (see, e.g., van Dokkum & Franx 1996). Figure 6 shows the offsets of our field galaxy sample in $\Delta \ln(M/L_B)$ as

Images at www.strw.leidenuniv.nl/~vdwel/private/FPpaper/

FIG. 3.— Color images and $r^{1/4}$ -profile fit residuals of the early-type galaxies used in the analysis in the subsequent sections. The color images of the objects in the CL1252 field consist of i and z band images, the color images of the objects in the CDFS consist of v , i and z band images. The residuals are shown in the z band for all objects. The boxes are $5''.4$ on a side. The residual images are not distortion corrected, which causes the small dissimilarities between the color and residual images. The numbers at the upper left and right of the residual images are, respectively, the symmetric and asymmetric fluxes in the absolute residuals within two effective radii, expressed as percentages of the total fluxes of the galaxies within the same radius.

FIG. 3.— Continued

Images at www.strw.leidenuniv.nl/~vdwel/private/FPpaper/

FIG. 4.— Color images and $r^{1/4}$ -profile fit residuals of the galaxies with late-type or irregular morphologies. These galaxies have measured velocity dispersions but are not included in the analysis in the subsequent sections. For an explanation of the images and the numbers, see Figure 3.

a function of redshift. The values are listed in Table 3. Cluster samples from the literature are also shown. The galaxies in our sample seem to evolve faster than the galaxies in the cluster samples, and the scatter in $\Delta \ln(M/L_B)$ is large. Before we interpret the scatter and the apparent difference between field and cluster galaxies, we need to investigate the origin of the scatter. In Figure 7 we show M/L_B as a function of the rest-frame $B-I$ color. Galaxies with low M/L are bluer than galaxies with high M/L , as expected from the stellar population models shown in the figure. In Figure 8 we show a similar relation between rest-frame $U-B$ and M/L_B , but in this case the correlation is less clear, due to the fact that the range of $U-B$ colors is much smaller than the range of $B-I$ colors, and probably also because $U-B$ is more sensitive to small variations in the star formation history. Considering the correlation between color and M/L and the fact that M/L evolves with redshift, one expects that color evolves with redshift as well. In Figure 9 we show $B-I$ as a function of redshift; note the strong similarities between Figures 6 and 9. The strong correlation between color and M/L , and the similarity in M/L evolution and color evolution confirm that the observed evolution and scatter of M/L are intrinsic, and not due to measurement errors.

We calculate the evolution of M/L of our field sample by performing a linear fit and minimizing the mean deviation, weighting by the inverse of the error, and forcing the fit to go through the $z = 0.02$ data point derived from the Faber et al. (1989) sample. We separately consider the evolution of the primary sample, which contains the galaxies satisfying all of our selection criteria. We find that the average evolution of our entire early-type galaxy sample is $\Delta \ln(M/L_B) = (-1.75 \pm 0.16)z$ ($(-1.72 \pm 0.15)z$ for the primary sample alone), which is significantly faster than the evolution found for cluster galaxies, which is $\Delta \ln(M/L_B) = (-1.28 \pm 0.08)z$ (van Dokkum & Franx 1996; Kelson et al. 2000, van Dokkum & Stanford 2003; Wuyts et al. 2004, Holden et al. 2005). The scatter in $\Delta \ln(M/L_B)$ is 0.58 for our field galaxy sample (0.54 for the primary sample), and 0.28 for the MS1054 cluster sample (Wuyts et al. 2004).

Figure 5 suggests that the M/L evolution may depend on galaxy mass, as galaxies with small r_{eff} and low σ tend to lie lower with respect to the local FP as compared to galaxies with large r_{eff} and high σ . This was also found for cluster galaxies by Wuyts et al. (2004). We estimate M and M/L in solar units as described by van Dokkum & Stanford (2003).

The values are listed in Table 3. We explore the mass dependence by color coding the galaxies in Figure 6 according to their masses. Red points are galaxies with masses larger than $M = 2 \times 10^{11} M_\odot$; blue points are galaxies that have masses lower than $M = 2 \times 10^{11} M_\odot$. There is a striking difference between low and high mass galaxies. For galaxies with masses $M > 2 \times 10^{11} M_\odot$ we measure $\Delta \ln(M/L_B) = (-1.20 \pm 0.18)z$ for our field sample and $(-1.12 \pm 0.06)z$ for the cluster samples. For the massive galaxies in the primary sample alone we find $\Delta \ln(M/L_B) = (-1.26 \pm 0.18)z$. The observed scatter is decreased to 0.34 for the field sample (0.32 for the primary sample), and to 0.28 for the cluster samples. When changing this mass cut to $3 \times 10^{11} M_\odot$, as is done by Wuyts et al. (2004), but thereby limiting the number of galaxies in our sample to four, we find $(-1.12 \pm 0.13)z$ and $(-0.99 \pm 0.10)z$ for our sample and the cluster samples, respectively. We conclude that for high-mass galaxies, there is no difference between the cluster samples and our field sample. The galaxies with masses $M < 2 \times 10^{11} M_\odot$ in our sample evolve much faster: $\Delta \ln(M/L_B) = (-1.97 \pm 0.16)z$ ($(-1.90 \pm 0.17)z$ for the primary sample alone). We verify that these results do not change if galaxies with spectra with $S/N < 12$ are included as well. Therefore, the accuracy of our results is not limited by the quality of the velocity dispersions.

In Figures 6 and 9 we show evolutionary tracks for a single stellar population for formation redshifts $z = 1$ and 2. This very simple model assumes that luminosity evolves with time as $L \propto (t - t_{form})^\kappa$, where κ is derived from stellar population models (see van Dokkum et al. (1998) for more details). These tracks indicate a large spread in formation redshifts. We note, however, that κ is sensitive to the IMF. Here we use a single stellar population from Bruzual & Charlot (2003) with a Salpeter IMF and solar metallicity, which yields $\kappa = 0.97$ in the B band and 0.43 in the I band. According to this model the massive galaxies have high luminosity weighted formation redshifts ($z \geq 2$), whereas less massive galaxies in our sample have lower formation redshifts ($1 < z < 2$).

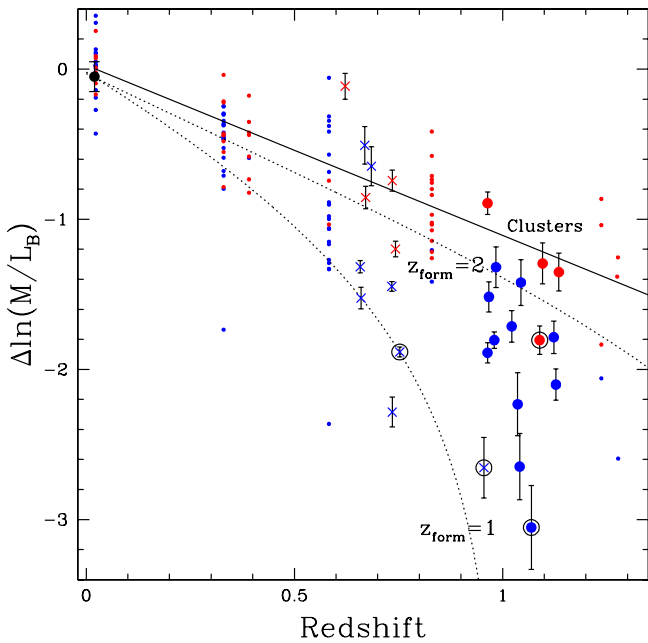


FIG. 6.— The offset from the local FP in the rest-frame B band for individual cluster galaxies taken from the literature (small dots) and the early-type galaxies with high S/N spectra in our sample. We distinguish, as in Figure 5, between the primary sample (filled symbols) and the fillers (crosses). The red symbols are galaxies with masses $M > 2 \times 10^{11} M_{\odot}$. The blue symbols are less massive galaxies. The cluster samples are taken from Jørgensen et al. (1996), Kelson et al. (2000), van Dokkum & Franx (1996), Wuyts et al. (2004), Holden et al. (2004), and van Dokkum & Stanford (2003). The solid line is $\Delta \ln(M/L_B) = 1.12z$, which is the best fitting straight line for the evolution of cluster galaxies with masses $M > 2 \times 10^{11} M_{\odot}$. The dotted lines are model tracks for a single stellar population with formation redshifts 1 (lower line) and 2 (upper line) (see text for a more detailed explanation). These model tracks are forced to go through the black point at $z = 0.02$ which represents the field galaxies in the sample of Faber et al. (1989). The range in offsets from the local field FP is large, but there is a strong correlation with mass. Massive field galaxies evolve as fast as equally massive cluster galaxies, while less massive galaxies evolve faster.

4.3. The relation between M and M/L and the role of selection effects

Figure 10 illustrates the tight relation between mass and M/L_B . We also show the SDSS field sample described in Section 4.1. The M/L of all galaxies have been corrected for evolution as derived from massive cluster galaxies, $\Delta \ln(M/L_B) = -1.12z$.

At $z = 1$, the relation between M/L and M seems much steeper than in the local universe. However, we have to take selection effects into account. Since we selected our sample in the z band, we can transform our magnitude limit into a luminosity limit in the rest-frame B band, which is close to the observed z band at $z \sim 1$ (the median redshift of our sample of 16 $z \sim 1$ galaxies is $z = 1.04$). Because this luminosity limit only applies to our primary sample, this discussion does not involve the fillers (mainly galaxies at $z \sim 0.7$). Afterward, we will comment on these galaxies.

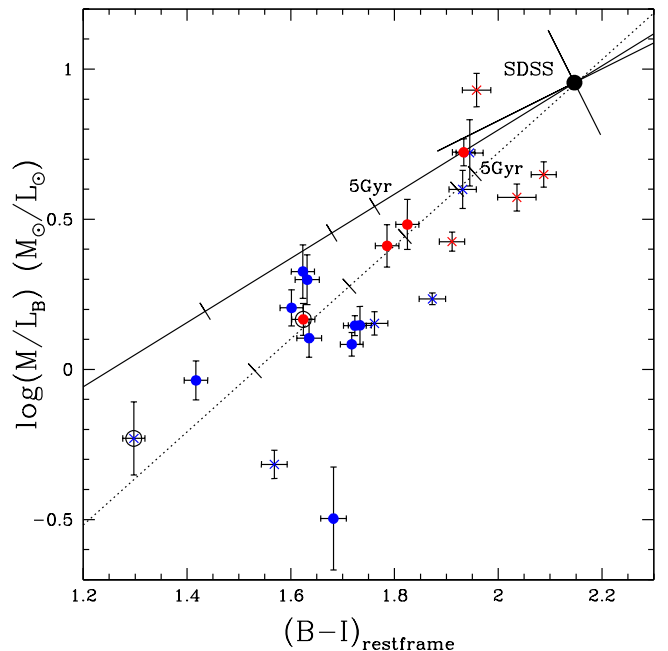


FIG. 7.— Rest-frame $B-I$ color versus M/L_B for our early-type galaxy sample. For an explanation of the symbols, see Figure 6a. The large symbol at the upper right indicates the median $B-I$ and M/L_B of the massive galaxies ($M > 2 \times 10^{11} M_{\odot}$) in the SDSS field early-type galaxy sample. The orientation of the distribution around the median values and the amount of scatter are indicated by the tilted error bars. The dotted line is a solar metallicity Bruzual-Charlot model for a single stellar population. The solid line is a model with exponentially declining star formation ($\tau = 1$ Gyr). Both model tracks are shifted vertically to match the SDSS data point. Model ages are indicated by ticks at intervals of 1 Gyr. The correlation between M/L and color implies that the observed scatter in M/L is real, and can be ascribed to age differences between the stellar populations of the galaxies. Our $i-z \geq 0.86$ color selection limit roughly corresponds to $B-I \geq 1.1$ according to the Bruzual-Charlot models. This shows that our selection criterion only excludes galaxies with ages less than 1 Gyr, and does not affect our conclusions regarding the massive, red galaxies.

We first test whether the observed distribution can be fully explained by selection effects, assuming that the slope and the scatter of the FP do not evolve. The probability that the observed distribution is drawn from a population with the same distribution as the SDSS galaxies is 0.14%, if the M/L evolution is the same for all galaxies. Therefore, the slope evolves, the scatter evolves, or both. If there is an age difference between high and low mass galaxies, the scatter will most probably also evolve differently for high and low mass galaxies. We cannot exclude with high confidence that the observed distribution of M/L is due to a larger scatter at high redshift: if the scatter in M/L at $z = 1$ is twice as large as in the local universe, the probability of a non-evolving slope is 8.0%. However, we see no evidence for an increase in the scatter at the high mass end, where selection effects do not play a role. Hence, if the scatter evolves, this is only true for galaxies with masses $M \sim 10^{11} M_{\odot}$. Since the increased scatter is most likely caused by young ages, low mass galaxies would have lower M/L , and hence the slope of the relation would also be changed. We consider these findings as strong evidence for mass-dependent evolution of early-type galaxies. To confirm that we observed a change in the slope of

the FP, deeper and larger surveys are needed.

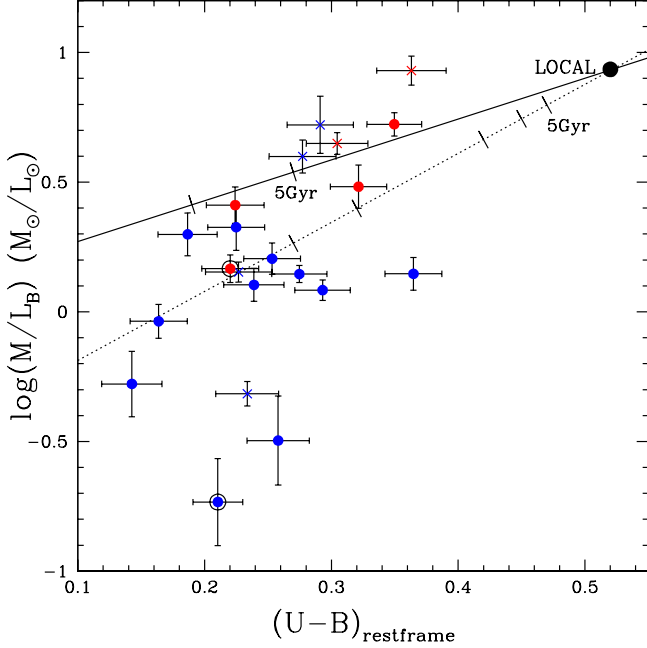


FIG. 8.— Rest-frame $U-B$ color versus M/L_B for the early-type galaxy sample. For an explanation of the symbols, see Figure 6a. The 'Local' data point is taken from Gebhardt et al. (2003). There is a similar relation as in Figure 7, but it is less clear because the range of colors is much smaller in $U-B$ than in $B-I$. Our $i-z \geq 0.86$ color criterion corresponds to $U-B \geq 0.07$ at $z = 1$, which demonstrates that this criterion would only exclude the most extremely blue galaxies (with ages well below 1 Gyr).

The location of the luminosity limit at $z = 1$ in Figure 10 shows that our $z \sim 1$ sample is dominated by selection effects for masses $M < 6 \times 10^{10} M_\odot$. The objects which such low masses are only included in the sample because of their probably extreme M/L . We cannot correct the M/L of that subsample for the bias introduced by our luminosity limit.

On the other hand, for the sample of galaxies with higher masses, we can correct for selection effects, because they are relevant, but not dominant, as can be seen in Figure 10. The average evolution of the galaxies in the primary sample with masses $M > 6 \times 10^{10} M_\odot$ is $\Delta \ln(M/L_B) = (-1.55 \pm 0.16)z$. The median mass of this subsample of 12 galaxies is $M = 1.9 \times 10^{11} M_\odot$. We estimate the maximum bias by assuming that the slope is the same at $z = 1$ and in the local universe, but that the scatter is a factor two larger at $z = 1$ than at $z = 0$. In that case the observed distribution is expected to follow the short-dashed line in Figure 10. At a given mass, the difference between the solid line and the short-dashed line is the bias introduced by the selection effects in luminosity. We increase the observed M/L of each galaxy in our primary sample by the difference between the solid line and the short-dashed line at the mass of that galaxy. For galaxies more massive than $M = 2 \times 10^{11} M_\odot$ this correction is negligible, but for the galaxies with masses $M \approx 6 \times 10^{10} M_\odot$ this correction is about 30%. Using this method, we find a bias corrected evolution of the galaxies with masses $M > 6 \times 10^{10} M_\odot$ of $\Delta \ln(M/L_B) = (-1.43 \pm 0.16)z$. Given the uncertainty in the intrinsic scatter, deeper observations are necessary to confirm this value.

Besides a bias due to the luminosity limit, errors in the velocity dispersion produce correlated errors in M and M/L , hence underestimating the measured evolution. Taking the errors in σ into account, we find that this introduces a bias at the level of only 2-3%, which is several times smaller than our measurement accuracy.

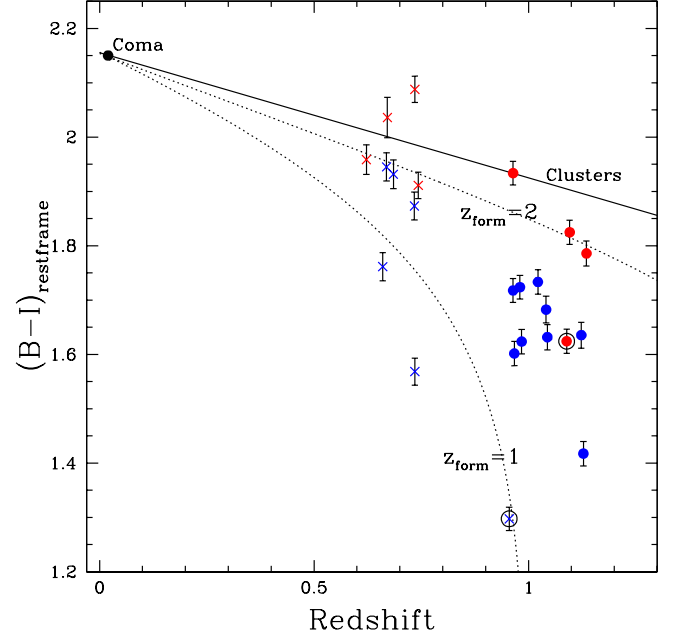


FIG. 9.— The evolution of the rest-frame $B-I$ color with redshift. For an explanation of the symbols, see Figure 6a. As already suggested by the tight relation between $B-I$ and M/L in Figure 7, the evolution of color with redshift is very similar to the evolution of M/L with redshift. Massive galaxies are the reddest in the local universe, and their color evolves slower than the color of low mass galaxies. Also, the color of the most massive field galaxies is very similar to the color of massive cluster galaxies.

The above analysis only involves $z \sim 1$ galaxies satisfying all our selection criteria, but we note that the relation between M/L and M exists for the $z \sim 0.7$ galaxies as well. However, this subsample is selected in an inhomogeneous way, therefore it is impossible to correct the observed evolution. Since all the galaxies roughly lie along lines of constant luminosity, the bias toward low M/L galaxies likely explains the observed relation between M and M/L for this sub-sample.

Besides by luminosity and morphology, the galaxies in our sample are also selected by color. This potentially introduces an important bias in the measured evolution, because of the exclusion of galaxies with blue colors, i.e., low M/L . Our color criterion, however, is quite generous. Even the very blue, low mass galaxies satisfy this criterion. For typical Bruzual-Charlot models, our color limit ($i-z = 0.86$) corresponds to $U-V \sim 0.67$ at $z = 1$, which is 0.2 mag bluer than the limit applied by Bell et al. (2004b) to select galaxies on the red sequence at $z \sim 1$. Our color cut is 0.45 mag bluer than the color-magnitude relation found by the same authors. From Bruzual-Charlot models we estimate that we only miss galaxies that are younger than ~ 1 Gyr (see Figures 7 and 8). Furthermore, Bell et al. (2004b) did not find blue, massive galaxies in the entire COMBO-17 dataset. Hence it is very unlikely that we miss any blue galaxy

at the bright end of our sample because of our color selection criterion.

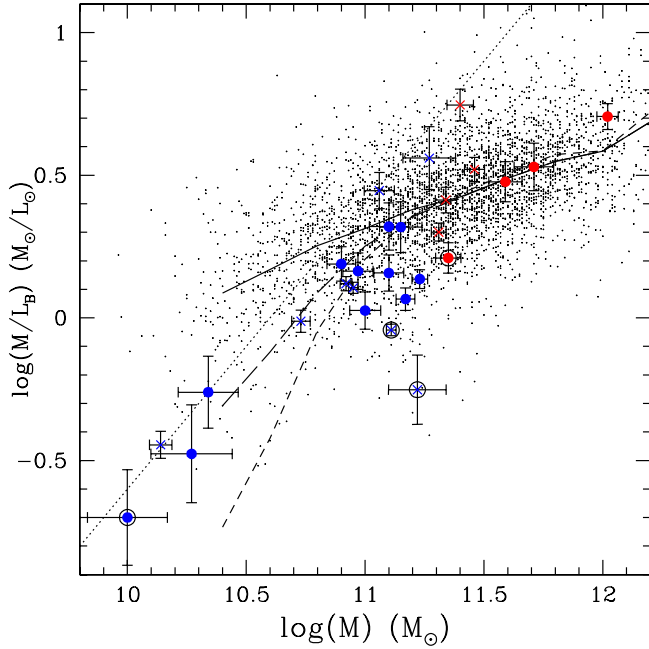


FIG. 10.— M versus M/L_B as derived from the FP for the early-type galaxies in our sample and for the nearby sample from the SDSS. For an explanation of the symbols, see Figure 6a. All data points have been corrected for M/L evolution as found for massive cluster galaxies, $\Delta \ln(M/L_B) = -1.12z$, normalizing at $z = 1$. The dotted line indicates our magnitude limit, translated into a luminosity limit at $z = 1$. Therefore, this limit only applies to the filled circles. The full drawn line indicates the median M/L_B of the SDSS early-type galaxies population. The long-dashed line indicates the median M/L_B of galaxies that are brighter than our luminosity limit at $z = 1$. Assuming that the scatter in M/L at $z = 1$ is a factor 2 larger than in the local universe, the median of the M/L of galaxies brighter than the luminosity limit follows the short-dashed line. It is clear that for the three galaxies in the primary sample with the lowest masses selection effects play such a dominant role that we cannot include these objects in our efforts to correct for this bias. Between $6 \times 10^{10} M_\odot$ and $2 \times 10^{11} M_\odot$ selection effects are relevant, but not dominant. For higher masses, selection effects do not affect our sample. The difference between galaxies with masses of $\approx 10^{11} M_\odot$ and masses $\approx 10^{12} M_\odot$ cannot be explained without an increase in the scatter with redshift, or assuming mass-dependent ages.

4.4. Independent evidence for mass-dependent evolution of early-type galaxies

It is particularly interesting to compare our results to the results from studies involving lensing galaxies, since those samples are mass selected. Rusin et al. (2003) and van de Ven et al. (2003) find $\Delta \ln(M/L_B) = (-1.29 \pm 0.09)z$ and $(-1.43 \pm 0.30)z$, respectively, using the same dataset. This seems somewhat low compared to the evolution of our sample and results found in the literature, but the lensing galaxies typically have high masses (see Table 4). The data for individual galaxies published by van de Ven et al. show that the median mass of the lens sample is $M = 2 \times 10^{11} M_\odot$, whereas the median mass of our early-type galaxy sample is $M = 1.3 \times 10^{11} M_\odot$. The galaxies in the lens sample that are more massive than $M = 2 \times 10^{11} M_\odot$ evolve

as $\Delta \ln(M/L_B) = (-1.13 \pm 0.31)z$. The galaxies less massive than this evolve much faster: $(-1.71 \pm 0.30)z$. The similarity between the results from the lensing sample and our sample is striking, especially because the lensing sample is mass selected. Hence, it is very hard to see how a bias toward low M/L galaxies can be responsible for the observed mass dependence in the lensing sample. It is possible that not all the low mass lenses are genuine early-types. If we omit the most irregular lenses (FBQ0951+2635, SBS1520+530, and B1608+656), we still find rapid evolution, $(-1.64 \pm 0.24)z$, for low mass lensing galaxies. Hence, these results provide strong evidence that the observed dependence of M/L evolution on mass in our sample is real. One possible complicating factor is that the lensing cross-section of galaxies in groups is larger than that of galaxies in the lowest density environments. This may lead to a difference between the populations of the lensing sample and our sample.

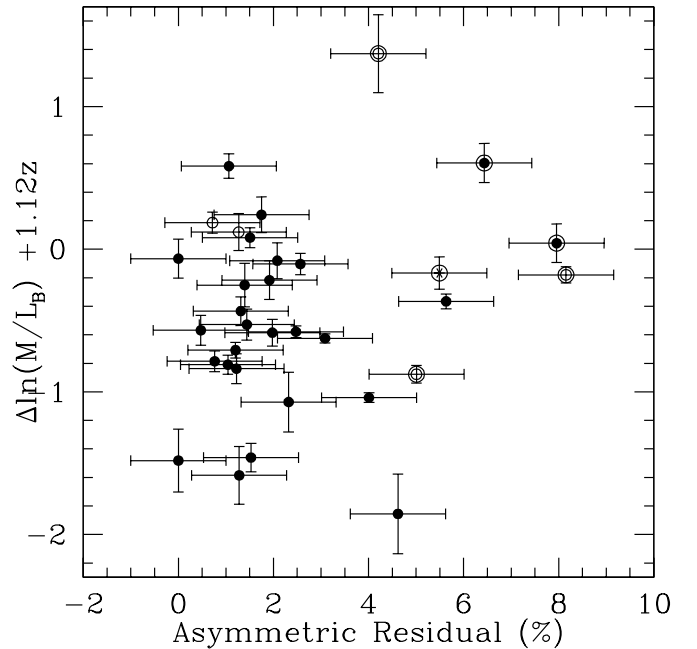


FIG. 11.— Asymmetric residuals of the $r^{1/4}$ -profile fits (see Figures 3 and 4) versus the offset from the local FP of the early-type galaxies in our sample, corrected for evolution. Filled circles are galaxies best fit with $r^{1/4}$ -profiles, asterisks with $r^{1/3}$, and open circles with $r^{1/2}$. Encircled objects are galaxies with late-type morphologies. A 2% or more residual indicates a significant deviation from symmetry in the light profile. There is no clear relation between M/L and deviations from smooth surface brightness profiles.

4.5. Ongoing star formation and morphological deviations

It is interesting to see that galaxies with emission lines have relatively low M/L , as can be seen from both Figure 6 and 10. Treu et al. (2002) have already shown that a substantial fraction of the massive early-type galaxy population at high redshift shows evidence for ongoing star formation by the presence of emission lines. Galaxies with emission lines in our sample, however, tend to have low masses. Figure 10 suggests that several of the galaxies with masses $\sim 3 \times 10^{10} M_\odot$ are included in the magnitude limited sample only because they are

forming stars. When excluding galaxies with emission lines, the evolution of the sample (without applying a mass cut), is $\Delta \ln(M/L_B) = (-1.61 \pm 0.18)z$. The galaxies with emission lines evolve faster: $\Delta \ln(M/L_B) = (-2.41 \pm 0.45)z$. On average, the mass of the galaxies without emission lines is 1.5 times larger than the mass of the galaxies with emission lines.

Mergers or interactions, accompanied with star formation, can lead to both deviations from smooth $r^{1/n}$ -profiles and low M/L values. van Dokkum & Ellis (2003) have shown tentative examples of this phenomenon. Figure 11 shows the magnitude of the asymmetric residual, (described in Section 3.1), versus the offset from the FP, corrected for luminosity evolution. There is no correlation between deviations from smooth surface profiles and M/L , and we find no evidence for a connection between star formation activity and interactions or mergers.

4.6. AGN

Four out of 11 early-type galaxies at $z < 0.8$ have AGN, and one out of 16 for the $z > 0.9$ sample, as determined from X-ray imaging (see section 3.3). Of the five early-type galaxies with AGN, three are more massive than $M = 2 \times 10^{11} M_\odot$ and two have emission lines in their spectra. The M/L evolution of galaxies in our sample with AGN is $\Delta \ln(M/L_B) = (-1.64 \pm 0.31)z$, which is not very different from the value for galaxies without AGN: $(-1.76 \pm 0.20)z$. However, the galaxies with AGN are twice as massive than the galaxies without AGN. Considering high mass galaxies only ($M > 2 \times 10^{11} M_\odot$), we find $(-1.46 \pm 0.24)z$ for galaxies with AGN and $(-1.02 \pm 0.41)z$ for galaxies without AGN. Now, the trend is reversed, but only one out of the five galaxies with an AGN has a particularly blue $B-I$ color for its M/L . Therefore, a larger sample is needed to confirm that the epochs of star formation and AGN activity are related. Woo et al. (2004) find that up to $z \sim 0.5$ the evolution of the FP for galaxies selected to have AGN is indistinguishable from otherwise selected galaxies. Our results provide tentative evidence that a difference may set in at higher redshift.

5. COMPARISON WITH PREVIOUS RESULTS

Various other authors have measured the M/L evolution of field early-type galaxies. In this section we compare these previous results with our findings, and we comment on the apparent inconsistencies that exist in the literature. In Table 4 we give the M/L evolution as reported by other papers, as well as the values we derive using the tabulated datasets given in those papers.

Treu et al. (2002) find $\Delta \ln(M/L_B) = (-1.66 \pm 0.31)z$. This number is corrected for selection effects, while the value in Table 4 is uncorrected, to make a fair comparison with other results. The median mass of the sample presented by Treu et al. (2003) is $2.5 \times 10^{11} M_\odot$ for a sample extending to $z \sim 0.6$. Tabulated data are only available for the lower redshift galaxies presented in Treu et al. (2001). Only the galaxies with very low redshifts ($z \sim 0.1$) have low masses, therefore the comparison between high and low mass galaxies cannot be made. We note that the evolution of the entire Treu et al. sample is consistent with the evolution of our entire sample, $(-1.75 \pm 0.16)z$, and that the evolution of the massive galaxies in our sample is only mildly inconsistent with the evolution of the Treu et al. sample. Several of the high mass galaxies in the Treu et al. sample have emission lines in their spectra, which contrasts with our sample.

Van Dokkum et al. (2001) find $(-1.35 \pm 0.35)z$ for an average redshift $z = 0.42$. The galaxy masses range from $3 \times 10^{10} M_\odot$

to $10^{12} M_\odot$ and are evenly distributed in $\log(M)$. Remarkably, when taking the tabulated data of the individual galaxies, and applying our fitting method, we find a larger value: $(-1.67 \pm 0.23)z$ (see Table 4). Van Dokkum et al. create redshift bins in which they calculate the bi-weight center of the M/L offset. This method is sensitive to the bin choice, which leads to the difference between the reported value and the value calculated with our fitting method. We note that, when using our fitting method, the result of van Dokkum et al. is very similar to the result presented in this paper. Splitting the van Dokkum et al. sample into low and high mass galaxies (at $M = 2 \times 10^{11} M_\odot$), we find $(-1.29 \pm 0.39)z$ for the high mass galaxies, and $(-1.94 \pm 0.34)z$ for the low mass galaxies. We verified that this 2.5σ difference can be explained entirely by the fact that the galaxies are luminosity selected, not mass selected. Contrary to this study and the work of Treu et al., van Dokkum et al. did not select the galaxies by color, but by morphology and magnitude only.

Van Dokkum & Ellis (2003) find $(-1.25 \pm 0.25)z$. The difference in fitting method, mentioned above, applies to this study as well. Additionally, their transformation from I -band surface brightness to rest-frame B -band surface brightness, using $V-I$ colors, is uncertain. Namely, using $V-I$ is an extrapolation for galaxies at $z > 0.8$. This leads to a different value for the M/L evolution if we use our method to fit to the individual galaxy data of the samples of van Dokkum et al. (2001) and van Dokkum & Ellis (2003): $(-1.69 \pm 0.13)z$, a value very similar to the result yielded by our sample. Using the bi-weight center to measure the evolution effectively gives very low weighting factors to outliers. If the two galaxies with the lowest M/L in the high- z sample of van Dokkum et al. are omitted, we find $(-1.53 \pm 0.13)z$. The measurement accuracy, together with the uncertain transformation to rest-frame properties can explain the remaining difference. The new sample described by van Dokkum & Ellis (2003) is too small to verify whether there is a trend with galaxy mass. There is one galaxy more massive than $M = 2 \times 10^{11} M_\odot$ with $\Delta \ln(M/L_B) = (-1.57 \pm 0.14)z$. As is the case for the sample of van Dokkum et al. (2001), the sample of van Dokkum & Ellis (2003) is not selected by color. This did not lead to faster evolution due to including blue early-type galaxies, which indicates that the color cuts in the other studies are adequately generous to avoid this bias.

Gebhardt et al. (2003) (hereafter G03) report a brightening in the rest-frame B band of early-type galaxies by 2.4 magnitudes at $z = 1$, which is derived from fitting a cubic spline to the offsets of the galaxies from the local FP. With our fitting method, we find $(-1.94 \pm 0.20)z$, using the data of the individual galaxies in that sample. This is consistent with the result presented in this paper. The difference between the value reported by G03 and our result using their data is caused by the three galaxies at redshifts $z > 0.9$. Our linear fit to their data and their fit agree well up to $z = 0.8$ (1.6 magnitudes brightening). If we split the G03 sample into high and low mass galaxies, we find an evolution of $(-1.59 \pm 0.50)z$ for galaxies more massive than $M = 2 \times 10^{11} M_\odot$, and $(-2.05 \pm 0.17)z$ for less massive galaxies. For low mass galaxies our result, $(-1.97 \pm 0.16)z$, and that of G03 agree well. The fast evolution for massive galaxies in their sample remains unexplained, but given the large uncertainty and the small number of objects the inconsistency is only mild. We note, however, that contrary to the early-type galaxies in our sample, the early-type galaxies in the G03 sample do not show a correlation between M/L and rest-frame $U-B$

color. One of the galaxies in the G03 sample serves as an example of the uncertainty. HST14176+5226 has been observed spectroscopically before (Ohyama et al. 2002) and happens to be in the sample of lensing galaxies of Rusin et al. (2003) and van de Ven (2003). G03 give a stellar velocity dispersion of $\sigma_* = 222 \pm 8 \text{ km s}^{-1}$ corrected to the same aperture as our dispersions. Ohyama et al. have measured $\sigma_* = 245 \pm 15 \text{ km s}^{-1}$, also corrected to the same aperture, which implies a somewhat smaller offset from the local FP. van de Ven et al. report a value of $\sigma = 292 \pm 29 \text{ km s}^{-1}$ as derived from the lensing model. The latter value leads to a rate of evolution that we find for the massive galaxies in our sample. Repeated observation of these massive galaxies may be illuminating.

We conclude that all the results found in the literature are mutually consistent, once differences in calculating and presenting the results have been taken into account.

6. CONCLUSIONS

We obtained ultra-deep spectroscopy for 27 field early-type galaxies with redshifts $0.6 < z < 1.15$. The offset of these high redshift galaxies from the local FP is used as a measure of the evolution of M/L and as an age estimator.

The average evolution of the early type galaxies in our sample is $\Delta \ln(M/L_B) = (-1.75 \pm 0.16)z$. The value we find for galaxies in the primary sample, those galaxies satisfying all our selection criteria, is the same. The scatter in $\Delta \ln(M/L_B)$ is large: 0.58. This shows that some galaxies must have high luminosity weighted formation redshifts ($z > 2$), while others have formed a large fraction of their stars at redshifts $1 < z < 2$. Emission lines in the spectra indicate that some galaxies show signs of ongoing star formation at the epoch of observation. This is in agreement with the presence of massive early-type galaxies with emission lines at $z \sim 0.5$ Treu et al. (2002), although the galaxies with emission lines in our sample tend to have low masses.

We find a tight correlation between M/L and rest-frame color, which shows that the variation in M/L among the galaxies in the sample is intrinsic, and due to differences in the stellar populations. The galaxies in our sample span a large range of masses. We find that low mass galaxies have larger offsets from the local FP than high mass galaxies. Because luminosity selected samples are biased toward galaxies with low M/L this is a trend that is expected. We carefully analyze whether the observed correlation between mass and M/L can entirely be explained by this selection effect or not. We find that galaxies with masses $M < 6 \times 10^{10} M_\odot$ are only included in our sample because they have low M/L . For galaxies at $z \sim 1$ with masses larger than $M = 6 \times 10^{10} M_\odot$, our sample is biased, but to a limited amount. Taking into account the selection effect, we exclude with high confidence that the distribution of mass and M/L of our $z \sim 1$ galaxy sample with masses $M > 6 \times 10^{10} M_\odot$ has the same distribution as the low redshift field early-type galaxy sample taken from Bernardi et al. (2003), corrected for evolution. We do not claim that we have observed a change of the slope of the FP, because we cannot exclude the possibility that our sample is drawn from a distribution that has the same slope as the Bernardi et al. sample, but with a scatter that is twice as large at $z = 1$. However, the outliers do not occur at the high mass end ($M \sim 10^{12} M_\odot$) of our galaxy sample, but at lower masses, namely $M \sim 10^{11} M_\odot$. Therefore, our results show that the evolution of early-type galaxies is mass-dependent, whether by an increase in the scatter at lower

masses, or by systematic faster evolution of lower mass galaxies as compared to higher mass galaxies, or, which is the most natural explanation, by a combination of these effects. Assuming the scatter has decreased from $z = 1$ to the present day by a factor of 2, we find that the for bias corrected M/L evolution of $z \sim 1$ early-type galaxies with masses $M > 6 \times 10^{10} M_\odot$ is $\Delta \ln(M/L_B) = (-1.43 \pm 0.16)z$.

Previous studies (Treu et al. 2001, 2002; van Dokkum et al. 2001, van Dokkum & Ellis 2003, Gebhardt et al. 2003), that claimed to have derived mutually exclusive results, are in fact consistent with our results, if the same fitting method is applied to the different datasets. Particularly interesting is the consistency of our results with the results from a sample of lensing galaxies (Rusin et al. 2003; van de Ven 2003), which also shows the mass-dependence, even though this sample is not biased toward galaxies with low M/L : because of the selection technique, the lens sample contains galaxies with typical M/L at a given mass. Our luminosity limited sample is sensitive to outliers, which are present indeed. The combination of these independent results strengthens the evidence for mass-dependent evolution and the combined increase in both slope and scatter with redshift.

Bell et al. (2004) claim that the mass density of red sequence galaxies increases by at least a factor of 2 from $z \sim 1$ to the present. This is partly based on the observation that the luminosity density is constant out to $z = 1$. The M/L evolution of our galaxy sample implies an increase by a factor of 4 in the mass density. In the local universe, most of the mass density in early-type galaxies is accounted for by galaxies with a velocity dispersion of $\approx 225 \text{ km s}^{-1}$ (Kochanek et al. 2000) or a mass of $\approx 3 \times 10^{11} M_\odot$. If those galaxies, which evolve somewhat slower, dominate the evolution of the mass density, the increase is slightly less (3–3.5).

The correlation between mass and M/L has been observed in clusters as well (Wuyts et al. 2004), but this can entirely be explained by selection effects. Both our field sample and the cluster samples found in the literature are not strongly biased for galaxy masses $M > 2 \times 10^{11} M_\odot$. When applying this mass cut, the evolution for cluster galaxies is $\Delta \ln(M/L_B) = (-1.12 \pm 0.06)z$, and the evolution for field galaxies is $\Delta \ln(M/L_B) = (-1.20 \pm 0.18)z$ ($-1.26z$ for galaxies in the primary sample). Galaxies with masses comparable to the mass of L^* galaxies in the local universe ($\approx 3 \times 10^{11} M_\odot$) have luminosity weighted ages that imply formation redshifts $z \geq 2$, independent of environment. If progenitor bias is important, the luminosity weighted age of typical early-type galaxies in the local universe can be considerably lower.

In hierarchical formation models, the predicted difference between the M/L of field and cluster galaxies is $\Delta \ln(M/L_B) = 0.55$, independent of redshift (van Dokkum et al. 2001). This large difference is related to the difficulty of constructing isolated galaxies without active star formation, i.e. to the lack of a mechanism that truncates star formation from within the galaxy. Our results rule out this prediction at the 99.6% confidence level, up to $z = 1.1$.

Our findings are consistent with down-sizing (Cowie et al. 1996; Kodama 2004). This idea is independently corroborated by other observations, such as the decrease of the mass of 'E+A' galaxies with time (Tran et al. 2003), the lack of star formation in massive galaxies at redshifts $z \leq 1$ (De Lucia et al. 2004), the fossil record of star formation in local early-type galaxies (Thomas et al. 2004), and the claim of mass-dependent evolu-

tion of spiral galaxies (Ziegler et al. 2002, Böhm et al. 2004). The lack of age differences between field and cluster galaxies, and the suggested mass-dependent evolution of early-type galaxies show that individual properties of a galaxy, and not environment, play an important role in its formation.

We have shown that rest-frame optical colors can be used to measure galaxy masses at high redshift. This can be regarded as a step toward accurately calibrating SED fitting as a mass estimator. Certainly including Spitzer photometry in the rest-frame near-infrared will provide tight correlations between dynamically derived M/L and M/L derived from SED fitting. Line-strengths of absorption features in our high S/N spectra will connect low redshift fossil record studies to evolutionary studies such as these, and constrain the metallicity

range of early-type galaxies at $z \sim 1$, lifting the age-metallicity degeneracy. Using the mass calibration for high-redshift galaxies, the evolution of the mass density and the mass function can be determined from volume limited samples. This will provide strong constraints on formation theories and the importance of progenitor bias.

We thank the referee for many useful comments, enhancing the quality and the readability of the work. We thank the ESO staff for their professional and effective assistance during the observations. The Lorentz center is thanked for its hospitality during various workshops and the Leidsch Kerkhoven-Bosscha Fonds for its financial support.

REFERENCES

- Alexander, D.M., et al. 2003, *AJ*, 126, 539
 Bell, E., McIntosh, D.H., Katz, N., & Weinberg, M.D. 2003, *ApJS*, 149, 289
 Bell, E.F., et al. 2004, *ApJ*, 608, 752
 Bernardi, M. et al. 2003, *AJ*, 125, 1866
 Bertin, E. & Arnouts, S., 1996, *A&AS*, 117, 393
 Blakeslee, J.P., et al. 2003, *ApJ*, 596, 143
 Böhm, A. et al. 2004, *A&A*, 420, 97
 Bruzual, A. G., Charlot, S. 2003, *MNRAS*, 344, 1000
 Cole, S., Lacey, S., Baugh, C.M., Frenk, C.S. 2000, *MNRAS*, 319, 168
 Coleman, G.D., Wu, C.-C., Weedman, D.W. 1980, *ApJS*, 43, 393
 Cowie, L.L., Songaila, A., Hu, E.M., & Cohen, J.G. 1996, *AJ*, 112, 839
 De Lucia, G. et al. 2004, *ApJ*, 610, L77
 Diaferio, A., Kauffmann, G., Balogh, M.L., White, S.D.M., Schade, D. & Ellingson, E. 2001, *MNRAS*, 323, 999
 Djorgovski, S. & Davis, M. 1987, *ApJ*, 313, 59
 Dressler, A., Lynden-Bell, D., Burstein, D., Davies, R.L., Faber, S.M., Terlevich, R., Wegner, G. 1987, *ApJ*, 313, 42
 Faber, S.M., Wegner, G., Burstein, D., Davies, R. L., Dressler, A., Lynden-Bell, D., & Terlevich, R. L. 1989, *ApJS*, 69, 763
 Kauffmann, G., Charlot, S. 1998, *MNRAS*, 279, L23
 Franx, M. 1993, *PASP*, 105, 1058
 Gebhardt, K. et al. 2003, 597, 239
 Giacomini, R., et al. 2002 *ApJS*, 139, 369
 Giavalisco, M. et al. 2004, *ApJ*, 600, L93
 Holden, B.P., et al. 2005, *ApJ*, in press, astro-ph/0412570
 Jørgensen, I., Franx, M. & Kjaergaard, P. 1995, *MNRAS*, 276, 134
 Jørgensen, I., Franx, M. & Kjaergaard, P. 1996, *MNRAS*, 280, 167
 Kauffmann, G., & Charlot, S. 1998, *MNRAS*, 297, L23
 Kelson, D.D., Illingworth, G.D., Franx, M., van Dokkum, P.G. 2000, *ApJ*, 531, 184
 Kochanek, C.S. et al. 2000, *ApJ*, 543, 131
 Kodama et al. 2004, *MNRAS*, 350, 1005
 Krist, J. 1995, in ASP Conf. Ser. 77, *Astronomical Data Analysis Software and Systems IV*, ed. R.A. Shaw, H.E. Payne, & J.J.E. Hayes (San Francisco: ASP), 349
 Lidman, C., Rosati, P., Demarco, R., Nonino, M., Mainieri, V., Stanford, S.A., Toft, S. 2004, *A&A*, 416, 829
 Ohya, Y et al. 2002, *AJ*, 123, 2903
 Rosati, P., et al. 2004, *AJ*, 127, 230
 Rusin, D. et al. 2003, *ApJ*, 587, 143
 Thomas, D., Maraston, C., Bender, R., & C. Mendez de Oliveira 2004, *ApJ*, in press
 Tran, K.-V., Franx, M., Illingworth, G.D., Kelson, D.D., & van Dokkum, P.G. 2003, *ApJ*, 599, 865
 Treu, T., Stiavelli, M., Bertin, G., Casertano, S., & Møller, P. 2001, *MNRAS*, 326, 237
 Treu, T., Stiavelli, M., Casertano, S., Møller, P. & Bertin, G. 2002, *ApJ*, 564, L13
 Valdes, F., Gupta, R., Rose, J.A., Singh, H.P., Bell, D.J. 2004, *ApJS*, 152, 251
 Vandame, B. et al., In Preparation
 van der Wel, A., Franx, M., van Dokkum, P.G., Rix, H.-W., 2004, *ApJ*, 601, L5
 van de Ven, P.M., van Dokkum, P.G., Franx, M. 2003, *MNRAS*, 344, 924
 van Dokkum, P.G. 2001, *PASP*, 113, 1420
 van Dokkum, P.G., Franx, M. 1996, *MNRAS*, 281, 985
 van Dokkum, P.G., Franx, M., Kelson, D.D., Illingworth, G.D. 1998, *ApJ*, 504, L17
 van Dokkum, P.G., Franx, M., Kelson, D.D., Illingworth, G.D. 2001, *ApJ*, 553, L39
 van Dokkum, P.G., Franx, M. 2001, *ApJ*, 553, 90
 van Dokkum, P.G., Ellis, R.S. 2003, *ApJ*, 592, L53
 van Dokkum, P.G. & Stanford, S.A. 2003, *ApJ*, 585, 78
 Wolf, C. et al. 2004, *A&A*, 421, 913
 Woo, J.H., Urry, C.M., Lira, P., van der Marel, R.P., and Maza, J. 2004, *ApJ*, in press
 Wuyts, S., van Dokkum, P.G., Kelson, D.D., Franx, M., Illingworth, G.D. 2004, *ApJ*, 605, 677
 Ziegler, B.L. et al. 2002, *A&A*, 364, 69

TABLE 1
COORDINATES OF THE GALAXY SAMPLE

ID	α J2000	δ J2000
CL1252-1	12:52:45.8899	-29:29:04.5780
CL1252-2	12:52:42.3588	-29:27:47.3112
CL1252-3	12:52:42.4793	-29:27:03.5892
CL1252-4	12:52:48.5594	-29:27:23.2452
CL1252-5	12:52:58.5202	-29:28:39.5256
CL1252-6	12:52:56.3846	-29:26:22.7868
CL1252-7	12:53:03.6396	-29:27:42.5916
CL1252-8	12:53:05.1228	-29:26:29.8680
CL1252-9	12:53:05.6213	-29:26:32.5608
CDFS-1	03:32:25.1597	-27:54:50.1332
CDFS-2	03:32:22.9265	-27:54:34.3429
CDFS-3	03:32:26.2940	-27:54:05.0411
CDFS-4	03:32:19.2880	-27:54:06.1445
CDFS-5	03:32:34.8486	-27:53:50.0705
CDFS-6	03:32:42.8569	-27:53:24.7700
CDFS-7	03:32:31.3700	-27:53:19.1519
CDFS-8	03:32:23.6062	-27:53:06.3463
CDFS-9	03:32:17.4796	-27:52:48.0004
CDFS-10	03:32:20.2801	-27:52:33.0150
CDFS-11	03:32:19.3006	-27:52:19.3400
CDFS-12	03:32:45.1488	-27:49:39.9558
CDFS-13	03:32:39.5987	-27:49:09.6024
CDFS-14	03:32:54.2299	-27:49:03.7722
CDFS-15	03:32:41.4049	-27:47:17.1409
CDFS-16	03:32:29.2152	-27:47:07.5718
CDFS-17	03:32:38.4940	-27:47:02.3640
CDFS-18	03:32:37.1944	-27:46:08.0663
CDFS-19	03:32:32.7124	-27:45:47.4617
CDFS-20	03:32:10.0387	-27:43:33.1237
CDFS-21	03:32:19.5922	-27:43:03.7848
CDFS-22	03:32:09.7051	-27:42:48.1090
CDFS-23	03:32:17.9117	-27:41:22.6795
CDFS-24	03:32:32.9855	-27:41:17.0102
CDFS-25	03:32:27.7000	-27:40:43.6865
CDFS-26	03:32:19.1468	-27:40:40.2190
CDFS-27	03:32:21.3600	-27:40:26.0861
CDFS-28	03:32:24.5444	-27:40:10.4322
CDFS-29	03:32:30.1945	-27:39:30.2407

TABLE 2
THE GALAXY SAMPLE

ID	e	X-ray	z_{spec}	S/N	σ km s ⁻¹	Type	r_{eff} ''	$\mu_{eff,z}$	z_{mag}	$i-z$	K_{mag}	$J-K$
CL1252-1	...	A	0.671	48	219 ± 12	K2	0.46	21.69	20.72	0.53	17.27	1.95
CL1252-2	0.658	75	216 ± 6	G2	0.18	20.04	20.35	0.46
CL1252-3*	$H\beta\gamma, [O III]$	A	0.844	83	166 ± 7	F6	1.04	22.78	19.30	0.54
CL1252-4*	[O III]	...	0.743	93	202 ± 8	F8	1.02	23.00	19.56	0.41	17.49	1.58
CL1252-5	...	A	0.743	61	251 ± 9	K1	0.36	21.07	19.91	0.53	16.98	1.81
CL1252-6	0.734	123	211 ± 5	G2	0.24	20.43	20.19	0.51	17.51	1.77
CL1252-7	[O II]	A	0.753	135	213 ± 5	G8	0.33	20.53	19.56	0.47
CL1252-8	[O II]	...	1.069	19	63 ± 13	F4	0.27	21.92	21.41	1.00
CL1252-9	1.036	18	102 ± 16	F8	0.22	21.71	21.59	0.88
CDFS-1	[O II]	A	1.089	27	231 ± 15	F4	0.44	21.97	20.36	1.12	17.70	1.83
CDFS-2	0.964	40	200 ± 9	G0	0.39	21.47	20.10	1.04	17.15	1.74
CDFS-3	1.044	17	300 ± 30	G4	0.15	20.39	21.14	1.07	18.29	1.75
CDFS-4	...	X	0.964	33	336 ± 18	G0	1.00	22.94	19.55	1.11	16.44	1.89
CDFS-5	0.685	32	194 ± 15	K1	0.37	21.64	20.42	0.66	18.27	1.81
CDFS-6	0.660	49	208 ± 9	G0	0.15	19.36	20.10	0.59	17.32	1.67
CDFS-7	1.135	17	232 ± 19	G4	0.74	23.32	20.58	1.14	17.26	1.97
CDFS-8	1.125	6	253 ± 70	G4	0.20	21.53	21.66	1.19	18.70	1.84
CDFS-9	1.097	8	215 ± 45	G0	0.21	21.20	21.21	1.22	18.09	1.86
CDFS-10	[O II]	...	1.119	9	275 ± 49	F6	0.091	19.68	21.50	1.10	18.72	1.70
CDFS-11	[O II]	...	1.096	10	208 ± 33	G2	0.23	21.87	21.67	1.23	17.93	1.9
CDFS-12	1.123	20	262 ± 20	G4	0.14	20.42	21.29	1.17	18.00	1.87
CDFS-13	0.980	46	247 ± 10	G4	0.20	20.93	20.17	1.05	17.22	1.83
CDFS-14	0.984	18	197 ± 21	G4	0.39	22.19	20.85	1.01	17.25	1.78
CDFS-15	0.622	55	317 ± 21	G8	0.31	20.94	20.09	0.62	17.41	1.73
CDFS-16	0.669	31	262 ± 36	G8	0.33	21.09	20.12	0.66	17.32	1.81
CDFS-17*	0.954	18	305 ± 31	F4	0.83	23.33	20.35	0.89	17.84	1.81
CDFS-18	1.096	14	324 ± 32	G0	0.51	22.21	20.3	1.20	16.98	1.92
CDFS-19	[O II]	...	0.955	15	229 ± 35	G4	0.34	20.35	19.30	0.49	17.53	1.56
CDFS-20	1.022	25	199 ± 15	G2	0.34	21.69	20.65	1.19	16.94	1.93
CDFS-21	0.735	56	149 ± 8	F4	0.073	18.52	20.81	0.56	18.05	1.59
CDFS-22	...	A,X	0.735	46	225 ± 11	K1	0.67	22.25	19.73	0.76	16.84	1.77
CDFS-23	1.041	13	70 ± 15	G4	0.39	22.59	21.23	1.09	18.51	1.77
CDFS-24*	...	A	1.042	25	210 ± 16	F8	1.87	24.35	19.60	0.96	17.10	2.00
CDFS-25	0.967	28	258 ± 18	F6	0.13	20.02	21.10	1.02	18.13	1.65
CDFS-26*	1.129	14	249 ± 25	G0	1.12	23.83	20.19	1.14	17.43	1.99
CDFS-27	[O II]	...	1.128	8	135 ± 30	F6	0.67	23.68	21.15	0.91	18.69	1.58
CDFS-28*	[O II]	A	0.954	12	445 ± 84	G4	0.80	23.54	20.64	0.80	18.52	1.78
CDFS-29	1.128	19	221 ± 17	F6	0.21	20.89	20.86	1.12	17.58	1.65

Note. — IDs labeled with an asterisk are late-type galaxies. An 'A' in the third column indicates an AGN, an 'X' indicates an extended X-ray source. The S/N in column 5 is in per Å (1.6 Å per pixel). σ is the aperture corrected central velocity dispersion measured with the best fitting stellar template. 'Type' indicates which spectral type fits best to the galaxy spectrum. The error on the effective radius may be taken from Table 3, which lists the physical sizes of the galaxies. $\mu_{eff,z}$ is the surface brightness in the z -band at the effective radius. The errors may be taken from the errors on the surface brightness in the rest-frame B -band, given in Table 3.

TABLE 3
PHYSICAL PARAMETERS OF THE GALAXY SAMPLE

ID	z_{spec}	$\log(R_{eff})$ kpc	$\mu_{eff,B}$ mag/arcsec ²	$\log(M)$ M_{\odot}	$\log(M/L_B)$ M_{\odot}/L_{\odot}	$\Delta \ln(M/L_B)$	$U-B$	$B-I$
CL1252-1	0.671	0.58 ± 0.02	23.64 ± 0.07	11.34 ± 0.04	0.57	-0.86 ± 0.07	0.68	2.04
CL1252-2	0.658	0.18 ± 0.02	21.92 ± 0.10	10.92 ± 0.02	0.29	-1.32 ± 0.04	0.61	...
CL1252-3*	0.844	0.88 ± 0.02	24.35 ± 0.05	11.39 ± 0.04	0.15	-1.82 ± 0.06	0.42	...
CL1252-4*	0.743	0.86 ± 0.01	24.61 ± 0.06	11.54 ± 0.03	0.54	-1.01 ± 0.06	0.52	1.67
CL1252-5	0.743	0.44 ± 0.02	22.80 ± 0.10	11.31 ± 0.03	0.43	-1.20 ± 0.05	0.68	1.91
CL1252-6	0.734	0.24 ± 0.02	22.17 ± 0.06	10.95 ± 0.02	0.23	-1.45 ± 0.03	0.62	1.87
CL1252-7	0.753	0.38 ± 0.01	22.17 ± 0.04	11.11 ± 0.02	0.08	-1.88 ± 0.03	0.47	...
CL1252-8	1.069	0.33 ± 0.05	23.39 ± 0.18	10.00 ± 0.17	-0.73	-3.05 ± 0.28	0.21	...
CL1252-9	1.036	0.25 ± 0.04	23.21 ± 0.16	10.34 ± 0.13	-0.28	-2.23 ± 0.21	0.14	...
CDFS-1	1.089	0.56 ± 0.05	23.41 ± 0.17	11.35 ± 0.05	0.17	-1.81 ± 0.09	0.22	1.62
CDFS-2	0.964	0.50 ± 0.03	23.10 ± 0.09	11.17 ± 0.04	0.08	-1.89 ± 0.07	0.29	1.72
CDFS-3	1.044	0.08 ± 0.05	21.89 ± 0.22	11.10 ± 0.08	0.30	-1.42 ± 0.15	0.19	1.63
CDFS-4	0.964	0.90 ± 0.02	24.58 ± 0.09	12.02 ± 0.04	0.72	-0.89 ± 0.07	0.35	1.93
CDFS-5	0.685	0.42 ± 0.04	23.59 ± 0.13	11.06 ± 0.06	0.60	-0.65 ± 0.13	0.28	1.93
CDFS-6	0.660	0.02 ± 0.02	21.26 ± 0.10	10.73 ± 0.04	0.15	-1.53 ± 0.07	0.23	1.76
CDFS-7	1.135	0.79 ± 0.04	24.69 ± 0.13	11.59 ± 0.07	0.41	-1.35 ± 0.13	0.22	1.79
CDFS-8	1.125	0.21 ± 0.09	22.93 ± 0.36	11.08 ± 0.21	0.37	-1.23 ± 0.37	0.26	1.62
CDFS-9	1.097	0.23 ± 0.05	22.62 ± 0.21	10.97 ± 0.16	0.10	-1.76 ± 0.26	0.33	1.77
CDFS-10	1.119	-0.13 ± 0.11	21.09 ± 0.43	10.82 ± 0.14	0.05	-1.86 ± 0.23	0.17	1.52
CDFS-11	1.096	0.27 ± 0.07	23.29 ± 0.29	10.98 ± 0.13	0.30	-1.30 ± 0.23	0.35	1.81
CDFS-12	1.123	0.06 ± 0.05	21.82 ± 0.22	10.97 ± 0.06	0.10	-1.79 ± 0.11	0.24	1.64
CDFS-13	0.980	0.38 ± 0.04	22.54 ± 0.15	11.23 ± 0.03	0.15	-1.81 ± 0.05	0.27	1.72
CDFS-14	0.984	0.49 ± 0.04	23.78 ± 0.22	11.15 ± 0.09	0.33	-1.32 ± 0.14	0.22	1.62
CDFS-15	0.622	0.32 ± 0.03	22.96 ± 0.13	11.40 ± 0.06	0.93	-0.11 ± 0.09	0.36	1.96
CDFS-16	0.669	0.36 ± 0.04	23.07 ± 0.16	11.27 ± 0.11	0.72	-0.51 ± 0.13	0.29	1.95
CDFS-17*	0.954	0.82 ± 0.05	24.93 ± 0.15	11.85 ± 0.08	0.87	-0.46 ± 0.14	0.15	1.64
CDFS-18	1.096	0.62 ± 0.03	23.63 ± 0.09	11.71 ± 0.08	0.48	-1.29 ± 0.14	0.32	1.83
CDFS-19	0.955	0.43 ± 0.03	21.84 ± 0.14	11.22 ± 0.12	-0.23	-2.66 ± 0.20	-0.32	1.30
CDFS-20	1.022	0.43 ± 0.05	23.24 ± 0.20	11.10 ± 0.06	0.15	-1.71 ± 0.11	0.36	1.73
CDFS-21	0.735	-0.28 ± 0.04	20.27 ± 0.14	10.14 ± 0.05	-0.32	-2.28 ± 0.10	0.23	1.57
CDFS-22	0.735	0.69 ± 0.03	24.21 ± 0.10	11.46 ± 0.04	0.65	-0.74 ± 0.07	0.30	2.09
CDFS-23	1.041	0.50 ± 0.05	24.10 ± 0.17	10.27 ± 0.17	-0.50	-2.65 ± 0.22	0.26	1.68
CDFS-24*	1.042	1.18 ± 0.05	25.86 ± 0.13	11.90 ± 0.06	0.48	-1.33 ± 0.11	0.08	1.47
CDFS-25	0.967	0.00 ± 0.08	21.63 ± 0.36	10.90 ± 0.06	0.21	-1.52 ± 0.10	0.25	1.60
CDFS-26*	1.129	0.96 ± 0.04	25.24 ± 0.11	11.83 ± 0.08	0.52	-1.22 ± 0.14	0.17	1.59
CDFS-27	1.128	0.74 ± 0.06	25.10 ± 0.17	11.07 ± 0.18	0.16	-1.62 ± 0.26	-0.06	1.34
CDFS-28*	0.954	0.80 ± 0.06	25.12 ± 0.18	12.17 ± 0.15	1.29	0.30 ± 0.27	-0.03	1.50
CDFS-29	1.128	0.24 ± 0.06	22.30 ± 0.20	11.00 ± 0.07	-0.04	-2.10 ± 0.10	0.16	1.42

Note. — IDs labeled with an asterisk are late-type galaxies. The rest-frame B -band surface brightness at the effective radius is corrected for cosmological surface brightness dimming. The error on M/L in solar units is the same as the error on M . $U-B$ and $B-I$ are rest-frame colors.

TABLE 4
COMPARISON WITH PREVIOUS RESULTS

Ref.	$\Delta \ln(M/L_B)/z$ reported	$\Delta \ln(M/L_B)/z$ fitted	$\Delta \ln(M/L_B)/z$ high mass	$\Delta \ln(M/L_B)/z$ low mass	$\langle \log(M/M_\odot) \rangle$	$\langle z \rangle$	N
Treu et al. 2001	-1.64 ± 0.12	-1.64 ± 0.34	-1.55 ± 0.27	-1.47 ± 1.89	2.3×10^{11}	0.29	19
van Dokkum et al. 2001	-1.35 ± 0.35	-1.67 ± 0.23	-1.29 ± 0.39	-1.94 ± 0.33	1.5×10^{11}	0.42	18
Treu et al. 2001, 2002	-1.84	2.5×10^{11}	0.38	29
van Dokkum et al. 2001, 2003	-1.25 ± 0.25	-1.68 ± 0.13	-1.41 ± 0.29	-1.77 ± 0.24	1.3×10^{11}	0.56	27
Gebhardt et al. 2003	-2.21	-1.94 ± 0.20	-1.59 ± 0.49	-2.05 ± 0.17	8.5×10^{10}	0.64	21
This paper	-1.75 ± 0.16	-1.75 ± 0.16	-1.20 ± 0.18	-1.97 ± 0.16	1.6×10^{11}	0.90	27
Rusin et al. 2003	-1.24 ± 0.21	0.54	21
van de Ven et al. 2003	-1.43 ± 0.30	-1.36 ± 0.18	-1.13 ± 0.31	-1.71 ± 0.30	2.3×10^{11}	0.54	21

Note. — Column 2 lists the values of the evolution of M/L as reported in the cited papers. Column 3 lists the values we derive using our fitting technique on the tabulated data of the individual galaxies in the cited papers. Column 4 lists the evolution of galaxies more massive than $M = 2 \times 10^{11} M_\odot$, using our fitting technique, and column 5 lists the evolution of less massive galaxies. Average masses, redshifts, and sample sizes (N) of the samples are also listed. When two references are given, the results presented in the newest paper are based on data of both papers. Treu et al. (2002) only list redshifts and velocity dispersions of the galaxies. The reported values are all uncorrected for selection effects. Treu et al. (2002) only give an error for the uncorrected value, and Gebhardt et al. (2003) do not give an error. Besides the magnitude limited samples, the two studies of the same sample of lensing galaxies are also listed. We only fitted the tabulated data from van de Ven et al. (2003), but the data presented by Rusin et al. (2003) yield the same results.